THE STUDY OF LOW LEVEL ACTIVITIES

Rb^{87}, V^{50}, Ta^{180}

A Thesis

submitted in partial fulfilment of

the requirements for the degree of

Master of Science

at the

University of Manitoba

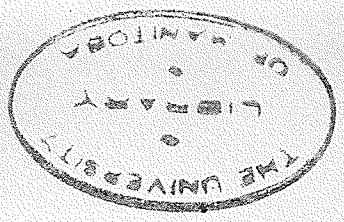

by

A. Petrau

August, 1956

TABLE OF CONTENTS

Page

LIST OF FIGURES

LIST OF TABLES

ABSTRACT

A scintillation spectrometer has been used to study the three naturally occurring radioactive isotopes: Rb^{87}, V^{50}, and Ta^{180}

Rb^{87}: The radioactive decay of Rb^{87} has been studied using the scintillations from a rubidium iodide, thallium activated, crystal. The beta-spectrum from 11.5 kev on has been obtained and an end-point energy of 275 kev is indicated. The allowed Fermi plot, forbidden in shape, has been extrapolated linearly to zero energy and a total counting rate of 1929 ± 65 counts per minute was obtained from 0.0938 gm RbI corresponding to a half-life of $(5.0 \pm .2) \times 10^{10}$ years. The shape of the spectrum has been fitted by several combinations of scalar and tensor interactions and the allowed Fermi plot linearized for the most part.

V^{50}: A specific search for the 1.58 Mev gamma radiation expected to follow K-capture in V^{50} to the first excited level of Ti^{50} has been made. Corrections for background distortion were attempted. Considerations of possible radioactive impurities in the sample have been taken into account. Calculations reveal that the half-life of V^{50} for this mode of decay is greater than 4.9×10^{14} years.

Ta^{180}: A picture, based on the single particle shell model, of the static properties of Ta^{180} has been proposed and a search for the 102 kev and 93 kev gamma rays, which should follow negatron emission and K-capture, respectively, has been made. A minimum half-life of 2.9×10^{12} years has been determined for either mode of decay. This does not agree with the theoretical picture proposed, indicating that the single particle shell model is inadequate in yielding a correct picture of the static properties of Ta^{180}. It is suggested that the unified model be used in determining these properties.

Chapter I

GENERAL INTRODUCTION

(i) General Survey: (1) (2) (3) (4)

The first evidence for the instability of nuclei in certain energy states, was the observation in the closing years of the past century, of the radioactivity of the heavy elements. In addition to alpha and gamma emission, radiations consisting of negatively charged particles were observed in many cases. By the measurement of their e/m value, for instance, these particles have been identified as electrons. With the advent of the artificial production of radioactive nuclei this phenomenon of beta emission has been shown to be very wide spread. There are very few mass values corresponding to which there is not at least one beta-radioactive isobar.

In addition to negative electron emission two other kinds of beta-radioactive processes, positron emission and orbital electron capture are known. All three of these closely related processes are known collectively as beta decay; for each process the mass number A remains constant. The process of negatron and positron emission may be represented by:

$$Z^A \longrightarrow (Z \pm 1)^A + \beta^{\mp} + \nu \qquad (1.1)$$

where ν represents an accompanying neutral particle. On the other hand the orbital electron capture is represented by:

$$Z^A + e^- \longrightarrow (Z-1) + \nu \qquad (1.2)$$

Generally speaking the lifetimes for the beta-process are very long; measured half-lives vary from a fraction of a second to 10^{14}

years or more. The slow processes are associated with large angular momentum changes between the nuclear states involved, as well as with parity changes.

Epistemologically, beta-decay in nuclear physics is important for two reasons. By measuring the shape of the beta spectrum information about the angular momentum and parity changes involved in the transition can be obtained. This is significant in determining the static properties of the parent and daughter nuclei. Secondly, the beta-decay process presents a new type of interaction in physics. The form is similar to that of the electromagnetic interaction in the process of emission and absorption of light quanta. Unfortunately, the beta-decay process is considerably more complex and furthermore, there exists no classical theory that attempts to explain this type of interaction as fully as the electromagnetic interaction is explained by Maxwell's theory. Thus one has no guide to the study of the beta interaction.

The neutral particle mentioned in equation (1.1) and (1.2) was postulated by Pauli and utilized by Fermi in his attempt to formulate the first successful quantitative theory of the shape of the beta spectra and of the lifetime of the beta-ray emitters. Its existence was postulated in order to satisfy the basic principle that the process of beta-decay must satisfy the laws of conservation of energy, linear momentum, angular momentum, and statistics.

The beta-decay theory set up by Fermi is based on a mathematical structure which envisages the interaction as being due to the continuous absorption and re-emission by the nucleons of virtual electrons and neutrinos. When a real electron-neutrino pair appears a beta-emission has occurred(5). In the construction of the theory, the mathematical

form of the interaction as well as its strength, must be known. Several interaction forms which satisfy the physical and mathematical requirements are:(6)

S or scalar interaction .....H_S (a)

V or polar vector interaction.....H_V (b)

T or tensor interaction .....H_T (c) (1.3)

A or axial vector interaction.....H_A (d)

P or pseudoscalar interaction.....H_P (e)

The complete beta-interaction is a linear combination of the above; that is, the most general Hamiltonian for the beta-interaction is given by

$$H = C_S H_S + C_V H_V + C_T H_T + C_A H_A + C_P H_P \qquad (1.4)$$

The coupling coefficients C_x are constants whose values can only be determined by comparing theory with experimental results. Experimental evidence is currently regarded as having established the following points regarding possible combinations of the five forms of interactions:(8)

(i) The T and A forms must be a part of the correct law of beta-interaction. Only the T, or the A, form yields Gamow-Teller selection rules, which are needed for understanding the short lives of many beta- interactions with a unit spin change and no parity change.

(ii) The S or the V form must also be included. The chief evidence for this is the short life found for beta-transitions between nuclear states of zero spin.

(iii)* The P form is needed to explain the singular RaE spectrum.

Each of the above arguments require the inclusion of some component form without precluding the presence of other forms. A generally recognized empirical argument is that not both T and A forms, nor both the S and V forms, can be parts of the coupling. If they are, then the spec-

* Recently Yamada has shown that S,T(1-0) and V,A(1-0) fit the experimental data for the RaE Beta-spectrum, as well as T,P(0-0) if the finite De Broglie wave length effect is taken into account.
M. Yamada, Prog. of Theor. Phys. 10 , (1953) , 252 .

tra of allowed beta-emission should deviate from the allowed shape. However, no such deviations have been found. Also experimental evidence shows that C_V and C_A, rather than C_S and C_T, approximate zero.

(ii) The Allowed Energy Spectrum:

The detailed theory by which the energy spectrum is calculated for allowed transitions involves the evaluation of matrix elements arising from the general Hamiltonian for the beta-interaction. By considering only those transitions which have the largest decay constant, and hence the shortest half-life, the selection rules for allowed transitions are arrived at. They are:

$$S, V \quad \Delta J = 0 \quad \Delta \pi = no$$

$$T, A \quad \Delta J = 0, \pm 1, \; no \; 0 \rightarrow 0 \quad \Delta \pi = no$$

where J is the total angular momentum and π the parity. The energy spectrum for an allowed transition is given by:(7)

$$N\pm(W)dW = (g^2/2\pi^3)F(\mp Z,W)pW(W_o - W)^2C(M)^2(1 \mp b/W)dW \qquad (1.5)$$

where the rest mass of the neutrino is assumed to be zero, and $N\pm(W)dW$ is the fraction of the total number of processes with total electron energies between W and W+dW. The upper sign refers to positron and the lower to electron emission. $F(\mp Z,W)$ is a complicated function of Z and W. It describes the effect of the Coulomb field of the nucleus on the emitted electron. Its effect is to emphasize low-energy electrons and de-emphasize low-energy positrons, and is important for all but the lightest elements. Tables giving its value for a large range of values for Z as a function of p, the electron momentum, exist(45). The term $pW(W_o - W)^2$ represents the energy dependence of the distribution function for a pure interaction, that is, where there is no Coulomb field. It is called the statistical weight. It is derived on the basis of the number

of states available for the particles in momentum space. g^2 represents a coupling constant. The term b/W, referred to as the Fierz interference term, varies very slowly with W and is usually regarded as being effectively zero. The factor M in equation 1.5 is a nuclear matrix element. It is a measure of the probability of occurrence of the transition. Its value depends upon the type of interaction assumed and upon the wave functions of the nuclear particles before and after the process. Since little is known about the wave functions M can only be estimated. M fixes the order of the transition. It can be expressed as a series of terms, which if they do not vanish, become progressively smaller. The first term, if it does not vanish, is independent of energy. These transitions are what have here been called allowed transitions. C is a coupling constant which may be the sum of the squares of the coupling coefficients for scalar, tensor, etc. type of interaction. It gives an appropriately weighted mean of the square of the nuclear matrix element M.

Comparison of observed spectra with theory is usually made with the aid of the Kurie plot. With $b=0$ equation 1.5 may be written as:

$$N\pm(W)/F(\mp Z,W)pW^{1/2} = K(W_o - W) \qquad (1.6)$$

where K is now independent of the energy W. The modified Fermi function $G = pF(\mp Z,W)/W$ has been evaluated for a large range of Z values as a function of p, the electron momentum(45). With the aid of the observed energy distribution the quantity on the left may be computed and plotted against energy, W. For an allowed spectrum a straight line should be the result. However, it is often the case that there exists an upward curvature at the low energy end of the spectrum. This non-linearity at the low energy end has often been found to be attributable to distortions

introduced by self-absorption and scattering. The use of thinner sources and thinner backing materials has been found to improve the linearity of the allowed Kurie plot in some instances. On other occasions, however, the non-linearity of the allowed Kurie plot has not been corrected in this simple manner. It is then expected that the transition is not allowed.

(iii) Forbidden transitions:

In the theory of allowed beta-decay only transitions between nuclear states of the same parity and differing in spin by no more than one unit, are permitted. The allowed-transition selection rules arise after certain small effects are left out of consideration. These neglected effects become very important when their absence leads to a vanishing transition rate inasmuch as they then become responsible for the forbidden transitions.

The small effects neglected in the allowed theory are: (1) those due to corrections needed to produce Lorentz invariance in the vector, tensor, and axial vector Hamiltonians, (2) those arising from the variation of the lepton waves(electron and neutron waves) across the nucleus, and (3) those arising when the source velocity is not neglected. The source velocity effects are introduced by the requirement of Lorentz invariance for $H_{V,T,A}$ since the extra terms present in the Hamiltonians of these interaction forms are of the order v/c, where v is the nucleonic velocity. It is for this reason that these extra terms are referred to as "source velocity effects." When these velocity interactions are included, transitions which violate the allowed selection rules are generated and are referred to as forbidden transitions. When the variation of the lepton waves across the nucleus is considered the nuclear matrix element has to be expressed as a series of terms which become progressively smaller. The n^{th} term introduces n components of the moment arm

vector, $\underline{r}$, into the nuclear matrix element, giving rise to n^{th} forbidden transitions which may, or may not, be vanishingly small. The selection rules for the general, n^{th} forbidden transition are as follows:

$$\Delta J = n,\ n+1;\ \Delta\pi = (-1)^n \quad n \neq 1$$

$$\Delta J = 0,\ 1,\ 2 \quad \Delta\pi = -1 \quad n = 1$$

where $n=1$ corresponds to first forbidden transitions and $n \neq 1$ corresponds to second and higher order forbidden transitions. The selection rules for the allowed transitions have been given above.

The electron(negatron) spectrum for an n-times forbidden transition can be written as (9):

$$N_-(W)dW = (g^2/2\pi^3) F_o\ (+Z,W)\,(pW(W_o - W)^2\ S_n\ (W) \qquad (1.7)$$

in the notation used for the allowed spectrum. F_o here is defined as $F(Z,W)/(1+\gamma)/2$ where γ is equal to $\left[1 - (\alpha Z)^2\right]^{1/2}$, γ is the fine structure constant and Z, the atomic number. $S_n(W)$ is called the "shape factor" and is of considerable importance in that it is used as a means of linearizing the allowed Kurie plots of forbidden transitions. If $S_n(W)$ is independent of the energy W, then the spectrum has the "statistical shape" $\sim pW(W_o - W)^2$ modified only by the Coulomb effect, $F_o(Z,W)$. In general, however, $S_n(W)$ depends on the energy and a departure from the statistical shape is to be expected.

Several forms for the shape factor have been tried by various workers in the field but the one presented here and which will be used later, is the one developed by E. Konopinski(9). This shape factor, which is sometimes referred to as the "exact" shape factor, results from combinations of ST couplings.

The general, n-times forbidden shape factor can be written as the sum of two partial ones:

$$S_n = S_n^n + S_n^{n+1} \qquad (1.8)$$

S_n^n contributes to $\Delta J = n$ but not to $\Delta J = n+1$ transitions while S_n^{n+1} is the total shape factor for the " unique" forbidden transitions, $\Delta J = n + 1$. It also contributes to $\Delta J = n$ transitions (except for $J = 0 \rightarrow J = n$) but its contribution is negligible if the Coulomb energy $\propto Z/\rho$ is much greater than the maximum kinetic energy, $W_o - 1$. (ρ is the nuclear radius).

The partial shape factor S_n^n for negatron emission may be written as:(9)

$$S_n^n = \frac{4\pi n!}{(2n+1)!!} \sum \left| \int \beta \, \mathcal{Y}_{nm}(\underline{\sigma} \times \underline{r}) \right|^2 \times \left\{ C_T^2 P_n(\underline{\sigma} \times \underline{r}) + \right.$$

$$\lambda_n^2 (\alpha Z/2\ell)^2 C_T^2 P_n(\alpha) + \xi_n^2 C_S^2 P_n(\underline{r}) + \lambda_n (\alpha Z/\ell) C_T^2 I_n(\underline{\sigma} \times \underline{r}, \underline{\alpha}) +$$

$$\left. 2\xi_n C_S C_T I_n(\underline{\sigma} \times \underline{r}, \underline{r}) + \xi_n \lambda_n (\alpha Z/\ell) C_S C_T I_n(\underline{\alpha}, \underline{r}) \right\} \qquad \ldots(1.9)$$

where the η_n in Konopinski's notation has been changed to λn, to avoid confusing it with n. The functions P_n represent radiations by the individual "pure" moments, and the functions I_n are results of interference between the radiations(10). Both functions P_n and I_n depend on the emitted neutrino energy. The evaluation of these functions has been greatly facilitated by the work of Rose, Perry, and Dismuke(11), who have constructed exhaustive tables of data on the variables on which the functions are dependent. The real parameters ξ_n and λ_n are defined by:

$$\int(\beta) \mathcal{Y}_{nm}(\underline{\alpha}) = \lambda_n (\alpha Z/2\ell) \int(\beta) \mathcal{Y}_{nm}(\underline{\sigma} \times \underline{r})$$

and $$\int(\beta) \mathcal{Y}_{nm}(\underline{r}) = -i \xi_n \int(\beta) \mathcal{Y}_{nm}(\underline{\sigma} \times \underline{r}) \qquad (1.10)$$

respectively. Here $\int(\beta)\mathcal{Y}_{nm}(\underline{\alpha})$; $\int(\beta)\mathcal{Y}_{nm}(\underline{r})$ and $\int(\beta)\mathcal{Y}_{nm}(\underline{\sigma} \times \underline{r})$ are the spherical harmonic counterparts of the matrix elements:

$A_{i_1 \cdots i_n}$; $R_{i_1 i_2 \cdots i_n}$; $T_{i_1 \cdots i_n}$, respectively(9).

It is these real parameters that are manipulated in order to obtain the best possible fit between the experimental and theoretical Kurie plots for forbidden transitions. The usual procedure in testing a measured spectrum $N_-(W)$, as to whether it is governed by a given shape factor S, is to plot

$$\left[N_-(W)/S_n(W)F_0pW\right]^{1/2} \sim (W_0 - W) \qquad (1.11)$$

that is, one tries to linearize the spectrum with an appropriate choice of a theoretical shape factor.

(iv) Half-Life:

The total probability per unit time, λ, that a beta-active nucleus will decay is obtained by integrating $N_-(W)dW$, which is the probability of decay into a given energy interval dW, over the entire beta-spectrum. This probability also defines the half-life, t, of the beta-decay. We get:

$$\lambda = \frac{\ln 2}{t} = (g^2/2\pi^3)\int_1^{W_0} dW F_0\, pW(W_0 - W)^2\, S_n(W) \qquad (1.12)$$

This integral must be evaluated numerically. To do this for the spectrum of a general n-times forbidden transition requires that the shape factor $S_n(W)$ be known explicitly. This requires a numerical evaluation of the nuclear moments involved, as well as the scalar and tensor coupling coefficients, if the shape factor is of the form given by equation 1.9. Since little is known about nuclear wave functions the nuclear moments cannot at present be evaluated explicitly. The absolute magnitudes of the scalar and tensor coupling coefficients are not known but their relative strengths can be determined from analyses of allowed transitions (13). The present "best" value of

$$C_S^2/C_T^2 = 0.54^{+0.5}_{-0.25} \qquad (1.13)$$

Preston(42) suggests that from certain symmetry arguments the beta-decay interaction is S-T $\not$ P. Whether this implies a change in the relative strengths of the scalar and tensor coupling coefficients is not stated. In view of these difficulties in evaluating the integral of equation (1.12) it is re-written with $S_n(W) = 1$. Feenberg and Trigg(14) have given tables and graphs of the integral for the allowed beta-spectrum and these are usually used to obtain a numerical value of the integral in the general case.

From the definition of the half-life, $t = \ln 2 / \lambda$, it is clear that t is not in itself characteristic of an allowed transition since it is strongly dependent on the end-point energy W_o, of the beta-spectrum. On this account the half-lives of allowed transitions will show a wide variation. On the other hand the matrix elements associated with the scalar and tensor couplings C_S and C_T should be of the same order of magnitude for all allowed transitions. It is for this reason that the characteristic quantity, ft, called the comparative half-life, is calculated. The term f is the integral of equation 1.12 with $S_n(W) = 1$ and t is the half-life in seconds. For allowed transitions the values of ft cluster roughly into a single group. For forbidden transitions the ft values fall into distinct groups according to the order of forbiddenness of the transition. For the purposes of comparison, it is customary to take $\log_{10}$ft rather the ft. For the sake of completeness, a table giving the numerical values of $\log_{10}$ft for the different orders follows:

Transitions	$Log_{10}ft$
Allowed	4.5 to 6.0 for odd A 4.0 to 5.7 for even A
1 st. forbidden	6.4 to 7.3
2 nd. forbidden	12.2 to 13.5
3 rd. forbidden	17.5, 19

Although the ft value alone is not an infallible criterion on which a forbiddenness classification can be based, it plus a knowledge of the parity change is decisive since if the parity change is "no" the ambiguity exists between only two orders of forbiddenness, which differ by two units. The difference in the ft values for the two forbidden transitions is so large that no confusion as to the identity of the ft value can arise.

Chapter II

RUBIDIUM 87

(i) Review of the Literature:

That the isotope of rubidium with mass number 87 is radioactive, has been known for half a century, having first been discovered by J.J. Thomson(15) in 1905. It has also been separated from the other isotopes of rubidium by mass spectroscopy(16). The best value of 27.85% for its percentage abundance has been determined by A.O. Nier(17).

Since the time of discovery that Rb^{87} was naturally radioactive numerous determinations of its half-life have been made. In 1946 S. Eklund(18) measured the half-life with a counter calibrated by mixed alpha and beta particles from a uranium deposit. He found the half-life, t, to be 5.8×10^{10} years. The thinnest layer he used was 0.1 mg. RbCl/cm.^{2}. No coincidence between the particles emitted forward and those emitted backward was discovered, and thus it was concluded that the Rb^{87} decay involved the emission of a single particle.

In 1948 Haxel et al(19) measured very thin layers of RbCl produced by evaporation on silver coated Zapon foils of about 0.1 mg/cm^2, suspended freely between a counter arrangement which allowed the measure of particles from both sides of the foil simultaneously as well as the number of coincidences between counts on both sides. They found that with decreasing thickness of the RbCl layer from 2.0 to 0.05 mg RbCl/cm^2, the number of electrons per mg. RbCl per minute increased regularly for the back side of the foil, while the front side showed a considerably higher increase. This indicates a high percentage of very soft electrons from Rb, which could be stopped by the supporting Zapon foil. Coincidence measurements

indicated that up to 30% of the front side number for zero thickness coincided with counts on the back side. These results were explained by making the assumption that for every decay of Rb^{87} one soft electron of energy up to 10 kev is emitted as well as one faster electron with the known energy limit.

To check on the comparatively large error in measuring the exact amount of Rb deposited, Haxel et al(19) ran another series of experiments in which RbCl was evaporated on Al foils and placed on the inside wall of a GM counter of known efficiency. The weight of RbCl was accurately determined (3%) for a layer thickness of 0.025 mg/ cm^2 RbCl. Corrections for backscattering were made. As a weighted average of both series of experiments they obtained $(6.0 \pm 0.6) \times 10^{10}$ years for the half-life.

Curran et al(20) (1951), using a proportional counter, obtained an energy spectrum of the beta-disintegration from which they concluded that the process is simple beta-decay. The energy spectrum they obtained increases rapidly with decreasing energy down to at least 10 kev, which was the lowest point to which they pursued their observations. To verify that the decay process was simple in nature a search for K or L x-rays was carried out with the same equipment. As a further check a scintillation spectrometer was used to determine the number of events due to gamma emission. For an upper limit they obtained one gamma-quantum per 5×10^3 beta-rays. They concluded therefore that the process $Rb^{87} \longrightarrow Sr^{87} + \beta^-$ is a ground to ground-state transition and attributed the $\beta - e^-$ coincidence, reported by Haxel, as being due to reflection. For the half-life they obtained a value of $(6.15 \pm 0.3) \times 10^{10}$ years.

To re-evaluate the half-life and to provide further information about the decay scheme, MacGregor and Wiedenbeck(21) used a cell counter

described by Sawyer and Wiedenbeck(22). With the arrangement used the results were essentially independent of the decay scheme. For the half-life they obtained a value of $(6.23 \pm 0.3) \times 10^{10}$ years. In addition they carried out a series of experiments to determine whether or not there are coincidences between beta-particles and conversion electrons. The results obtained for Rb^{87} were compared with the results obtained for single beta-emitters having different upper energies such as Ni^{63} (50 kev) S^{35}(169 kev), Ca^{45}(260 kev), and P^{32}(1.7 Mev). They found that the coincidence curves for these elements varied slightly with the energy of the emitted radiation. The curves taken for the Rb^{87} sources of varying thickness were found to resemble most closely the curves for S^{35} and Ca^{45}. On the basis of these results they concluded that the disintegration of Rb^{87} consists of a simple beta-decay.

A more recent experiment making use of the latest advances in scintillation spectrometry, was carried out by Lewis(23). By using a crystal of rubidium iodide, activated with thallium, problems arising from self-absorption and back-scattering were avoided. However, new problems arising from poor resolution, low pulse height efficiency and long-lived phosphorescence inherent in the RbI(Tl) crystal, were introduced. The energy response of the crystal was found to be linear over the entire energy range from 17 kev on up. The beta-spectrum was then obtained by means of a single channel pulse height analyzer. The Fermi plot gave a forbidden shape, for the most part close to that given by Curran's(20) proportional counter work using 2π geometry, but having slightly more counts at the high energy end and fewer at the low energy end. The increase in the high energy counts was attributed to the fact that these particles are absorbed fairly completely in the crystal and not so well in the gas

counter. The fewer counts in the low energy end was attributed to the absence of back-scattering, as well as to the lower resolution of the crystal method at these energies. Upon extrapolating the allowed Fermi plot to zero energy and calculating the total counting rate, Lewis obtained a value of $(5.90 \pm 0.3) \times 10^{10}$ years for the half-life. Lewis attempted a theoretical analysis of the data and concluded that pure scalar interaction does not explain the Rb^{87} plot.

Perhaps the most thorough theoretical analysis of the Rb^{87} beta-spectrum has been carried out by Morita, Fujita, and Yamada(24). They have analyzed the experimental data of Lewis on the basis of the single particle shell model, in which case the beta-decay takes place with the transition of a neutron in a g9/2 state into a proton in a P3/2 state. On this basis the transition is third forbidden. In their analysis in terms of scalar and tensor interactions, there are four matrix elements to be considered. One of these, being a tensor of one rank higher than the others, is neglected because its effect is small. The two ratios formed by the other three appear as parameters; one ratio can be calculated on the single particle shell model or on the special j-j coupling shell model; the other is treated as a variable parameter whereby the Kurie plot is straightened out over the largest portion of its energy range. On the basis of their analysis they conclude that the sign of the ratio of the scalar and tensor interactions is probably minus; and its magnitude is somewhat smaller than unity.

The most recent work done on the beta-spectrum of Rb^{87} is that of Charles D. Goodman(25). He used a high pressure proportional counter with an internal source on a thin flat backing. No value of the half-life for the decay is given. In determining the beta-decay interaction Goodman

finds that the shape of the spectrum can be fitted approximately by several combinations of scalar and tensor interactions. However, lack of knowledge of beta-decay matrix elements prevents him from making a unique fit. In agreement with Morita, Fujita and Yamada, Goodman finds the ratio of C_S/C_T to be negative for the values of the matrix elements tried.

New emphasis on the importance of knowing accurately the half-life of Rb^{87} has been brought about by the recent development of the rubidium-strontium method of geochronometry(26). Since the calculation of a geologic age is based on a comparison of the extent of a transformation with the rate of the transformation it follows that the age is directly proportional to the assumed value of the half-life of the transforming nucleus. Therefore, the half-life must be accurately known.

Until recently, all reliable mineral ages seemed to be less than about 2.5×10^9 years. With the rubidium-strontium method of geochronometry, a number of ages close to this figure, and a few which exceed it substantially, have been obtained. Ahrens(46), who did not employ mass-spectrographic analysis, but who advanced good reasons for believing that lepidolites are usualy quite free of non-radiogenic strontium, obtained a number of apparent ages over 2×10^9 years for lepidolites. Some values, reported by other workers(29) using the same method of geochronometry, run as high as 3.36×10^9 years or higher. Some of the rocks tested have been analyzed as to their age by measurements based on the production of lead and helium by alpha- decay. In view of the fact that several ages derived from the decay of Rb^{87} are considerably greater than the upper limit for ages derived from alpha decay, and in view of the fact that the process of alpha disintegration is well understood, and that good minerals yield consistent ages by methods based on U^{238}, U^{235}, and Th^{232}, the suggestion

has been made that the currently accepted half-life of 6.2×10^{10} years for Rb^{87} is too large. Wetherill et al(47) have by determining the Rb^{87}/Sr^{87} ratio in samples of feldspar and mica by the mass spectrometric isotope dilution technique, calculated the half-life of Rb^{87} to be $(5.0 \pm .2) \times 10^{10}$ years on the basis of the Pb^{206}/U^{238} and Pb^{207}/U^{235} ages of uranium minerals taken from the same rock bodies.

It is for the purpose of investigating this possibility as well as seeking further information concerning the beta-decay interaction, that the Rb^{87} problem was attempted.

(ii) Apparatus:

1. The Scintillation Counter:

The electronic scintillation counter generally consists of a solid, liquid, or gaseous flourescent medium with a volume from a few cubic millimetres to as large as ten cubic feet. One or many photomultipliers are coupled to the phosphor to produce current pulses from the emitted light flashes. The shape and magnitude of the output current pulse obtained from the scintillation counters has been studied and found to be dependent to some extent on the following:First, the electrons arriving at the collecting anode of the photomultiplier tube do not arrive at precisely the same instant but are spread out over a time interval because the paths traversed by the individual electrons between multiplying stages are not identical and so different electrons have different transit-times between stages. This spread in the transit-time affects the resolution of the counter. Secondly, the photomultiplier output current waveform is dependent on the phosphor time-constant. If the decay time of the phosphor is very short, the output current waveform has both a sharp rise and a sudden drop. If, however, the phosphor exhibits a long decay-time the rise

time of the current pulse is slower and the pulse tends to have a long duration. In the case where the phosphor has both a phosphorescent and fluorescent component, the output current waveform is extremely long. In this case one may get both piling up of pulses, giving a higher number of the large amplitude pulses, and double pulsing, that is, where the decay-time of the fluorescent component is so much shorter than the decay time of the phosphorescent component, that the output current waveform of the photomultiplier has actually two maximum amplitudes. When this happens a paralysis circuit must be introduced into the differentiating circuit such that the circuit will be paralyzed for the duration of the phosphorescent component after it has passed the pulse due to the fluorescent component. This will be discussed more fully in a subsequent paragraph.

2. The Cathode Follower and Detector:

In a scintillation spectrometer the photomultiplier tube acts as a constant current source of high internal impedance. The current flows into, and is integrated by, the total stray capacitance of the tube output electrode and of the output circuit. This capacitance is shunted by the grid resistance of the cathode-follower tube (see figure 2.1) and a voltage waveform is obtained at high impedance. It is used to drive a cathode-follower tube, so giving a similar pulse at low impedance. The rise-time of the pulse is determined by the combined effect of the transit-time spread in the multiplier and the decay time-constant of the phosphor.

In the experiment about to be described the rubidium iodide thallium activated crystal used emitted both a fluorescent and phosphorescent component. It was due to the presence of the latter component that the output pulse of the standard cathode-follower was ragged and poorly integrated. The pulse observed from the crystal had a rise-time faster than one

microsecond, which is considerably longer than for phosphors most commonly used. To have a satisfactory integrating circuit as far as the main current pulse was concerned, the shunting resistance across the stray capacitance had to be increased to .5M from the usual value of 220K. To smooth out the raggedness of the pulse as much as possible a resistance of 4.7K was placed in series with the collecting anode of the multiplier. Larger resistance values attenuated the output pulse so much that any further improvement in smoothing out the pulse was not warranted. The introduction of an appropriate section of delay line in series with the collecting anode of the multiplier had a similar effect. A diagram of the photomultiplier and cathode follower is given in figure 2.1. Figures 2.2(a) and 2.2(b) give an indication of the smoothing out effect realized by the insertion of the 4.7K series resistance into the anode load of the photomultiplier.

The photomultiplier tube selected for the experimental work was a Dumont (Type K1190) with a cathode diameter of one inch. This tube was found to have the highest gain and at the same time, the lowest noise level of a dozen similar tubes tested. It was the same tube as the one used earlier in a series of radiocarbon dating experiments(27). Lewis's(23) pulse height analysis extended down to 17 kev below which the thermal noise level from his photomultiplier made further counting impracticable. With the K1190 photomultiplier it was expected that this analysis could be pursued below 17 kev.

3. Shielding:

The detector assembly was housed in a massive lead and mercury shield which was used to reduce the background counting rate to as low a value as possible without the use of anticoincidence shielding. A diagram of

FIGURE 2.1

PHOTOMULTIPLIER AND

CATHODE-FOLLOWER CIRCUIT

FIGURE 2.2

SHAPING OF OUTPUT PULSE

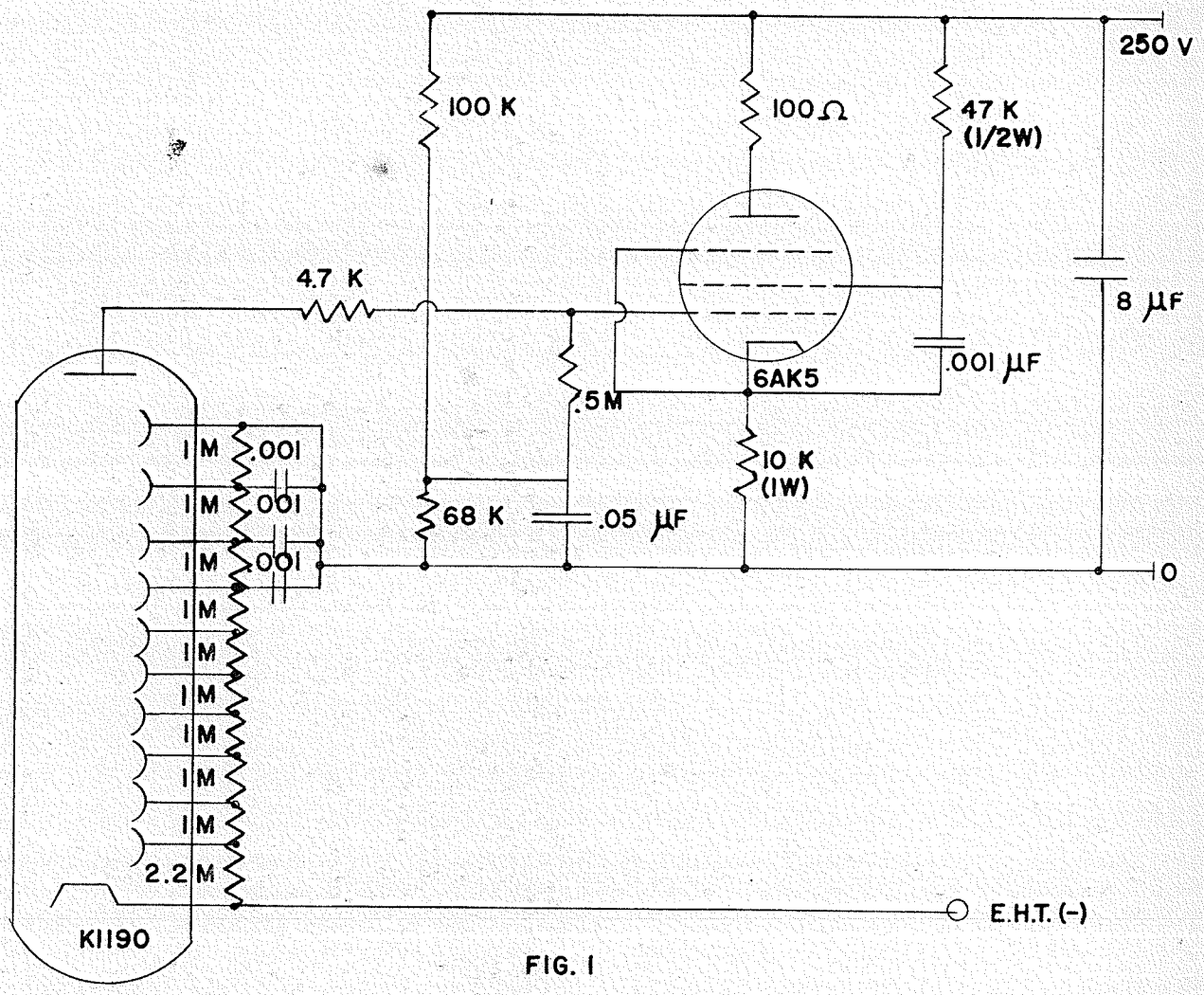
250 V
100 K
100 Ω
47 K
(1/2W)
4.7 K
8 μF
.001 μF
6AK5
.5M
10 K
(1W)
68 K
.05 μF
0
1 M
.001
1 M
.001
1 M
.001
1 M
1 M
1 M
1 M
1 M
1 M
2.2 M
K1190
E.H.T. (-)

FIG. 1

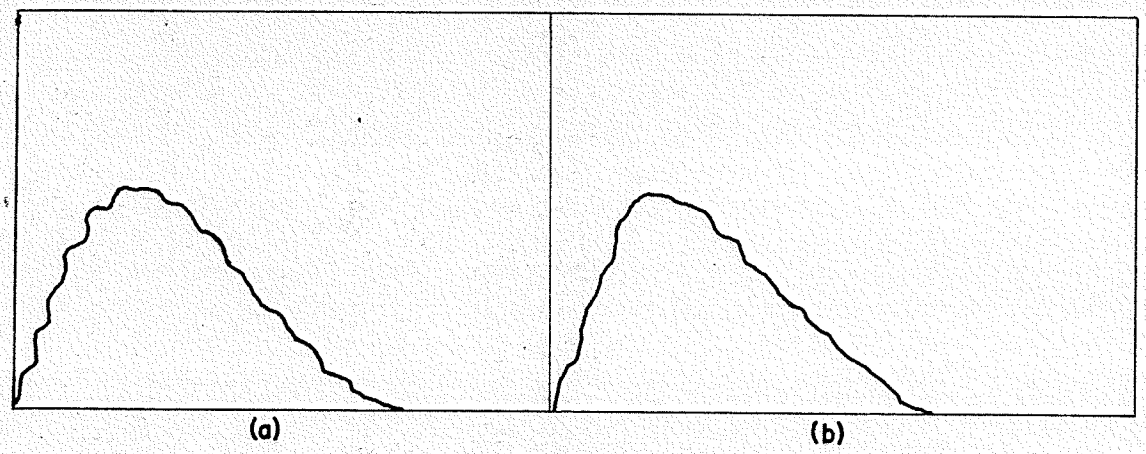
(a)
(b)

FIG. 2

the arrangement is given in figure 2.3. A fuller discussion of the effect of the shielding has already been given in previous work(28).

4. Electronics:

The pulses observed under gamma-bombardment were 1/12 th the height of those from thallium activated sodium iodide. Due to this low pulse height efficiency the demands placed on the amplifier were severe. The amplifier used was one that had been employed in past low-level counting apparatus. It is one of the Chase-Higginbotham 102 design and manufactured by the Radiation Instrument Company of Silver Spring, Maryland. It employs four long-tailed pair amplifiers plus a phase inverter and an output stage. The overall gain was determined to be about 40,000 or more. Considerable effort had to be made to eliminate to a large degree the ripple on the B-plus supply line. The noise level at full gain was reduced to an amplitude of three volts or less.

The pulse height analysis was carried out with a five-channel pulse height amplitude analyzer, manufactured by Murphy Radio Limited of England. The type 1074 has four contiguous differential gates and a surplus count channel whose discrimination level is contiguous with the top of the fourth channel. The channel width is adjustable from 0.25 to 5 volts, and the gates can scan a spectrum from 3 to 32.5 volts at the lowest level. In the analysis of the rubidium spectrum the gate width was varied in accordance with the overall gain required so that the energy interval over which a count was taken was kept constant. A detailed diagram of the unit is given in figure 2.3.

Lewis(23) reported that the rubidium iodide thallium activated crystal exhibited a phosphorescence decay lasting the order of a millisecond. As stated earlier, the way to avoid counting this radiation is

FIGURE 2.3

LOW LEVEL ACTIVITY

COUNTING APPARATUS

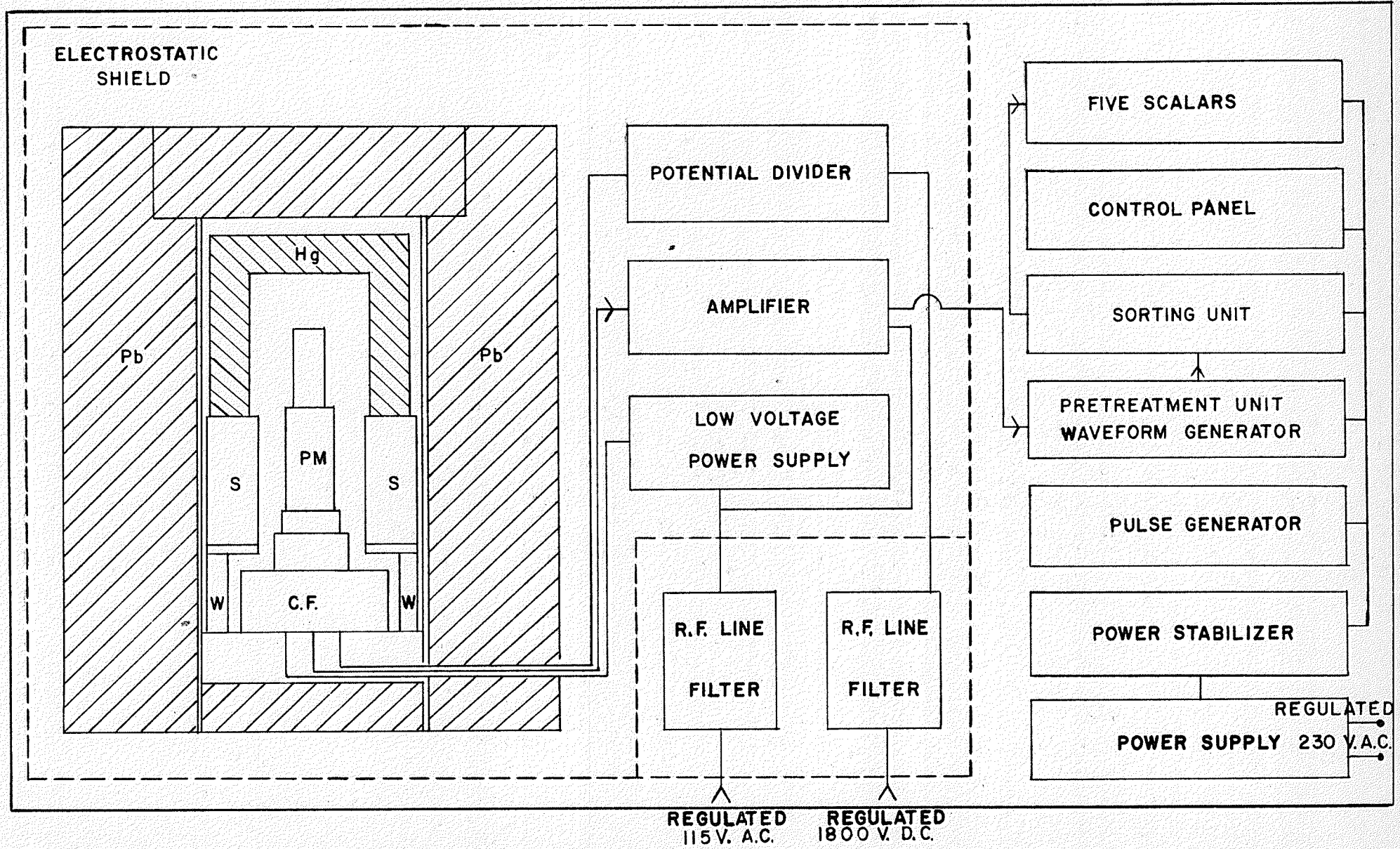
ELECTROSTATIC SHIELD
Hg
Pb
Pb
S
PM
S
W
C.F.
W
POTENTIAL DIVIDER
AMPLIFIER
LOW VOLTAGE POWER SUPPLY
R.F. LINE FILTER
R.F. LINE FILTER
REGULATED 115 V. A.C.
REGULATED 1800 V. D.C.
FIVE SCALARS
CONTROL PANEL
SORTING UNIT
PRETREATMENT UNIT WAVEFORM GENERATOR
PULSE GENERATOR
POWER STABILIZER
REGULATED POWER SUPPLY 230 V.A.C.

to use a paralysis circuit which will paralyze the discrimination circuit for the duration of the phosphorescence decay. A diagram of the paralysis circuit is given in figure 2.4. A description of its operation is briefly as follows: The paralysis circuit consists of a univibrator and a phase inverter operated by a separate Lambda type (Model 28) 300 volt stabilized power supply. The univibrator is triggered by the positive going pulse from the output of the pre-amplifier of the pre-treatment unit of the five-channel pulse height analyzer(point B). The positive pulse obtained from one of the plates of the univibrator is then inverted by the sharp-cutoff 6AU6 pentodes, two of which are required in parallel in order that the output pulse be of sufficiently large amplitude. The amplitude of the negative pulse was greater than 100 volts. This large amplitude pulse, whose length is variable by varying the value of the condenser C of the univibrator, is then applied through a high back-impedance crystal diode to the plate of the output tube of the long-tailed pair amplifier(point D). Upon testing the operation of the paralysis circuit with a pulse generator whose pulse could be varied both in repetition frequency and amplitude, it was found that the paralyzing circuit was fully effective, even in blocking out the large pulses when the smaller ones were being analyzed. Furthermore, the D.C. level of the discriminator was not affected.

5. Source and Background Materials:

For the source, a rubidium iodide thallium-activated crystal was obtained from G.M. Lewis, Department of Natural Philosophy, The University, Glasgow. Due to the irregularity of the crystal it was difficult to pack the MgO reflector around all free surfaces. Attempts were therefore made at flattening its sides by filing. However, due to its original small

FIGURE 2.4

PARALYSIS CIRCUIT

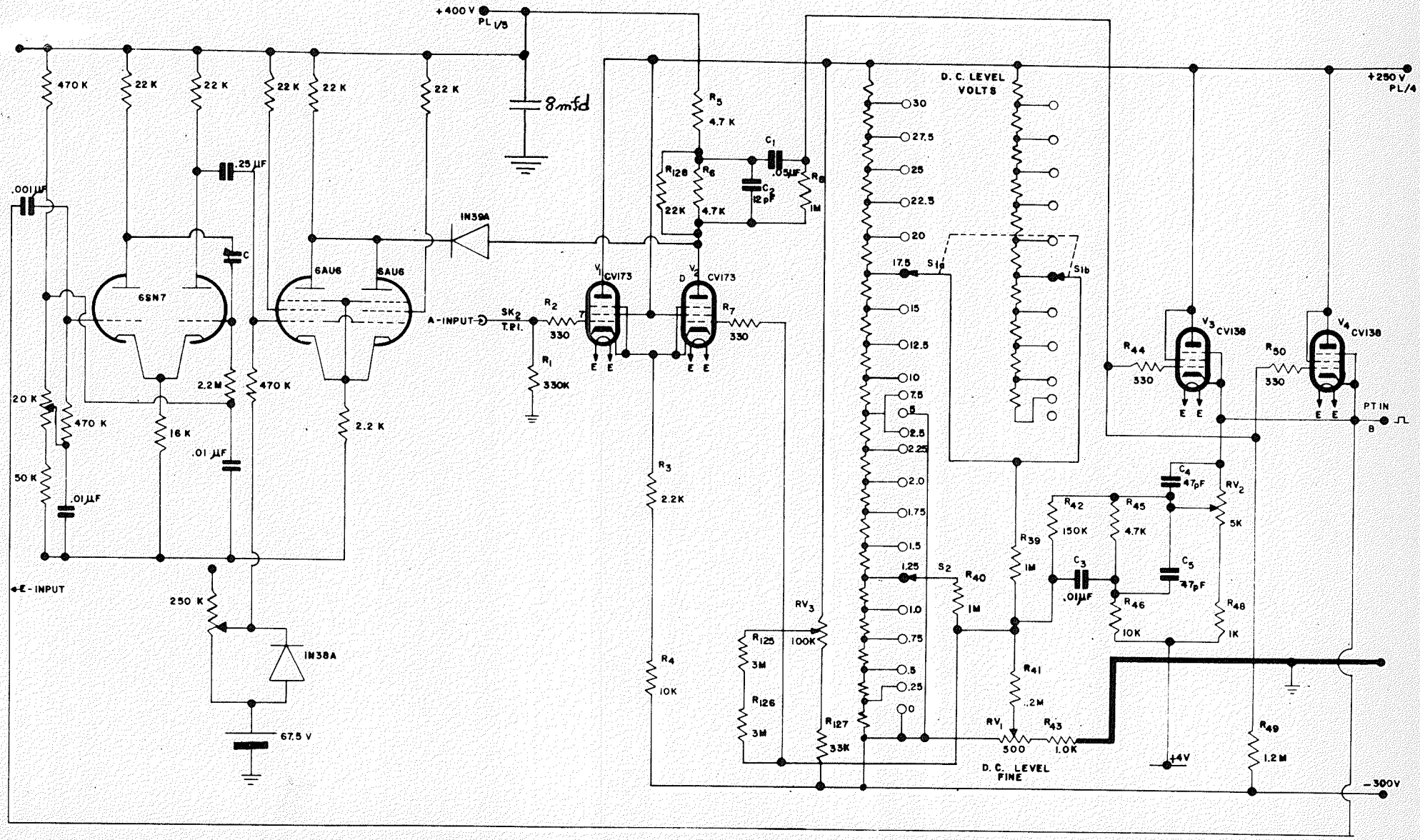
+400 V
PL 1/5
8 mfd
470 K
22 K
22 K
22 K
22 K
22 K
.25 µF
.001 µF
C
6SN7
6AU6
6AU6
IN39A
A-INPUT
SK2
T.P.I.
R2
330
R1
330K
V1 CV173
V2 CV173
R5
4.7 K
R128
22K
R6
4.7K
C1
.05µF
C2
12 pF
R8
1M
R7
330
R3
2.2K
R4
10K
20 K
470 K
50 K
.01 µF
16 K
2.2M
470 K
2.2 K
.01 µF
E-INPUT
250 K
IN38A
67.5 V
RV3
100K
R125
3M
R126
3M
R127
33K
D. C. LEVEL
VOLTS
30
27.5
25
22.5
20
17.5
15
12.5
10
7.5
5
2.5
2.25
2.0
1.75
1.5
1.25
1.0
.75
.5
.25
0
S1a
S1b
S2
R39
1M
R40
1M
R41
.2M
RV1
500
R43
1.0K
D. C. LEVEL
FINE
+14V
R49
1.2 M
-300V
+250 V
PL/4
V3 CV138
V4 CV138
R44
330
R50
330
PT IN
B
C4
47pF
RV2
5K
R42
150K
R45
4.7K
C3
.01µF
C5
47pF
R46
10K
R48
1K

size of about 4 mm. to the side, it was impossible to carry this process through to satisfaction. The upper side had to be left irregular. The crystal, as mounted, was approximately 4mm x 2mm x 3mm in dimension and weighed $0.0938 \pm .00005$ grams. For the container of the crystal a lucite ring, 3/4 inches outer diameter, 1/4 inch inner diameter, and 1/4 inch in height was made. Over one end a thin flat transparent glass was cemented. Using a little silicon grease for a bond, the small RbI crystal was mounted centrally in the ring with the flattened side next to the glass. MgO was then packed around the crystal from above, after which the top end was covered by a circular plate of plastic cemented to the ring. The crystal assembly thus formed could then be pút on and off the photomultiplier with ease. This was advantageous in view of the frequency with which the crystal had to be removed in order to determine the background counting rate.

To determine the background a NaI(Tl) crystal, of size similar to the RbI(Tl), was mounted in a container in a manner identical to that described in the preceding paragraph. Although the pulse height efficiency of the NaI crystal was twelve times greater than that of the RbI, the background could, nevertheless, be obtained in the same energy intervals by simply varying the overall gain of the electronic circuitry.

6. Calibrating Sources:

The pulse height scale at the high energy end was calibrated for energy in terms of the gamma radiation from Cs^{137} (662 kev) and I^{131} (364 and 284 kev). The 284 kev line was obscured for the most part by the large Compton effect due to the 364kev line. For a partial spectrum of I^{131} see figure 2.5. It is seen that the 80 kev line is well defined and that there is also good evidence of the 163 kev line. These plus the 46.5 kev line from RaD and the 31.5 kev Ba K x-ray were used to calibrate the middle part of the energy scale. Figure 2.6 shows the resolution ob-

FIGURE 2.5

PARTIAL SPECTRUM OF I^{131}

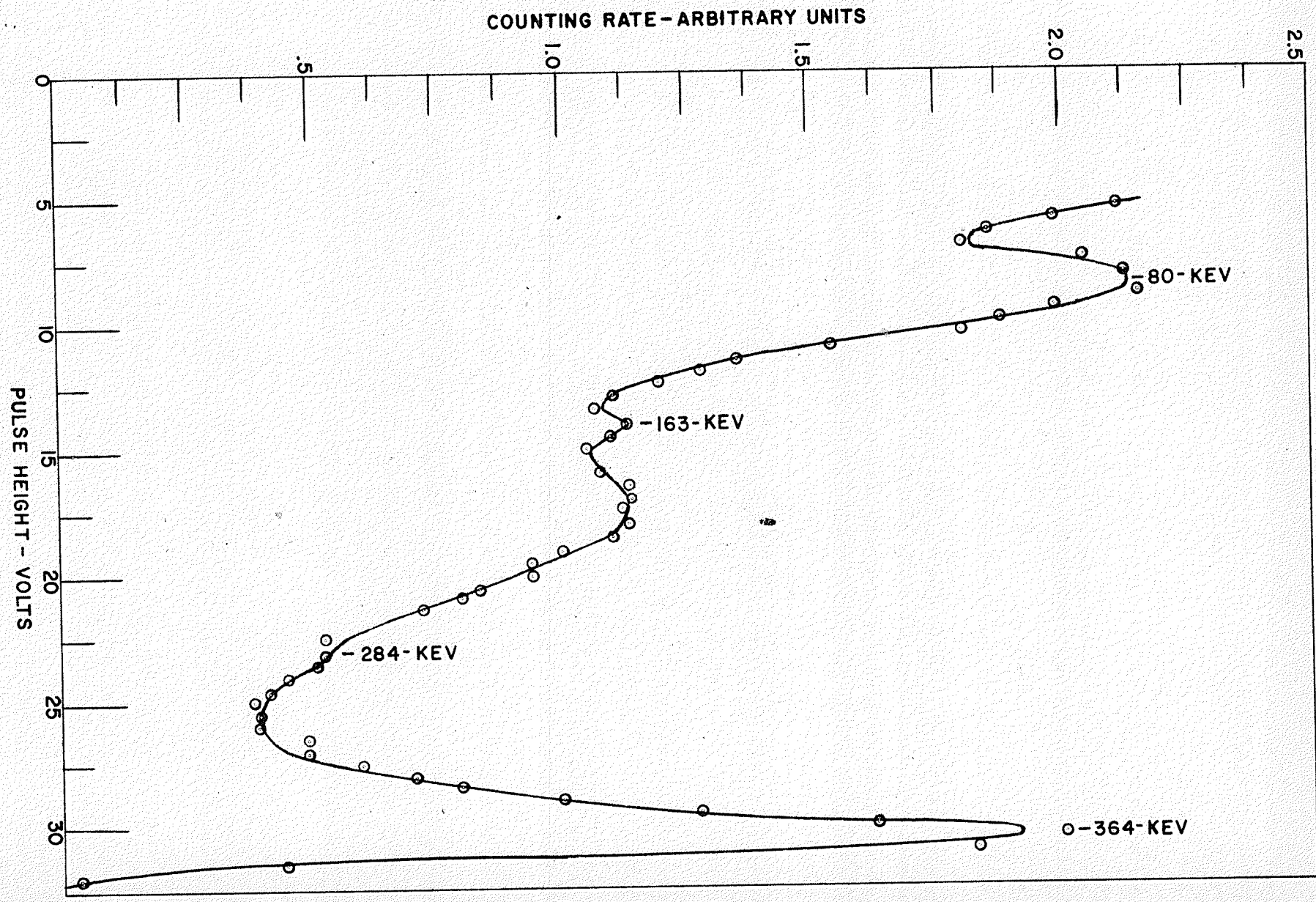
COUNTING RATE - ARBITRARY UNITS
0
.5
1.0
1.5
2.0
2.5
PULSE HEIGHT - VOLTS
5
10
15
20
25
30
80-KEV
163-KEV
284-KEV
364-KEV

FIGURE 2.6

RESOLUTION OF THE 46.5 KEV RaD

AND 31.5 KEV Ba K X-RAY

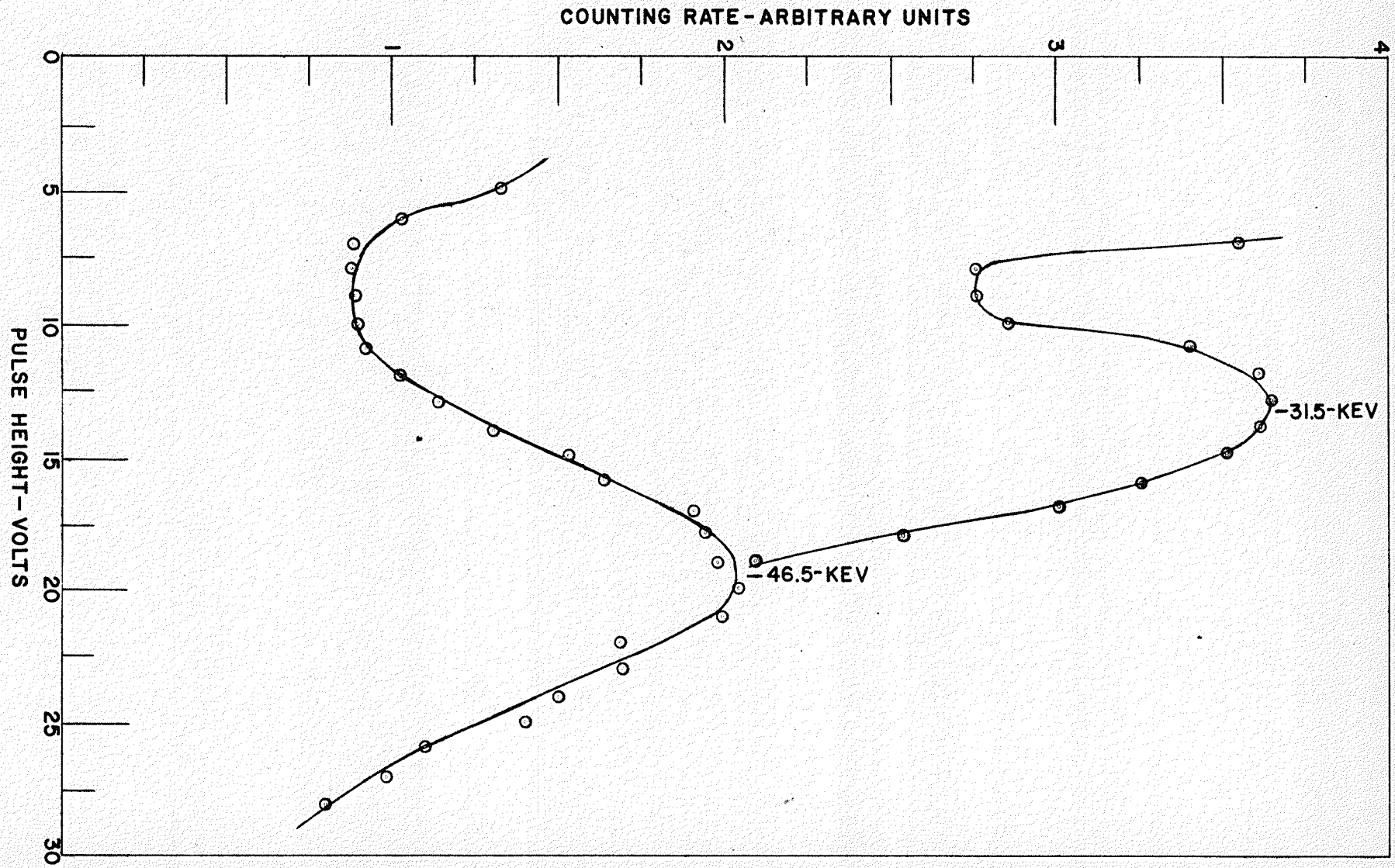
COUNTING RATE - ARBITRARY UNITS
0
1
2
3
4
PULSE HEIGHT - VOLTS
0
5
10
15
20
25
30
31.5-KEV
46.5-KEV

tained for the 46.5 kev RaD line and the 31.5 kev Ba K x-ray. The resolution was calculated as the ratio of the full width of a peak at half maximum to the mean amplitude of the peak. For the former it was 70% at 19.5 volts and for the latter 70% at 13.25 volts. With the small NaI(Tl) crystal the resolution of the two lines at comparable pulse heights was calculated to be 29.4% and 35%, respectively.

Lewis found that the pulse height vs. energy curve was linear over the range from 17 kev to 662 kev. To effect the calibration at 17 kev Lewis used the K x-rays of molybdenum. In this experiment, however, it was anticipated that a closer approach to zero of the energy axis could be made and a calibration point in the energy region 0 - 17 kev was therefore required. The K x-ray of Cu (7.8 kev), which follows orbital electron capture in Zn^{65} could not be resolved from the Compton component of the high energy part of the Zn^{65} spectrum. Therefore a germanium source was obtained from the Atomic Energy Commission of Canada. Ge^{71} decays wholly by electron capture to Ga^{71} and is followed by the production of Ga K x-rays. The 9 kev K x-rays were used for calibration. Figure 2.7 shows the resolution obtained at a pulse height of 11.5 volts. For full width at half-height it amounts to 82%.

During the pulse height analysis of the rubidium beta-spectrum the energy scale was calibrated before and after each run. With all the gammas or x-rays being reasonably intense this calibration took at the most a quarter of an hour.

7. Refrigeration:

In attempting to count in the energy region below 10 kev it was soon found necessary to reduce the photomultiplier tube noise by cooling. This was achieved by building a cylindrical jacket around the photo-

FIGURE 2.7

RESOLUTION OF 9KEV Ga K X-RAY

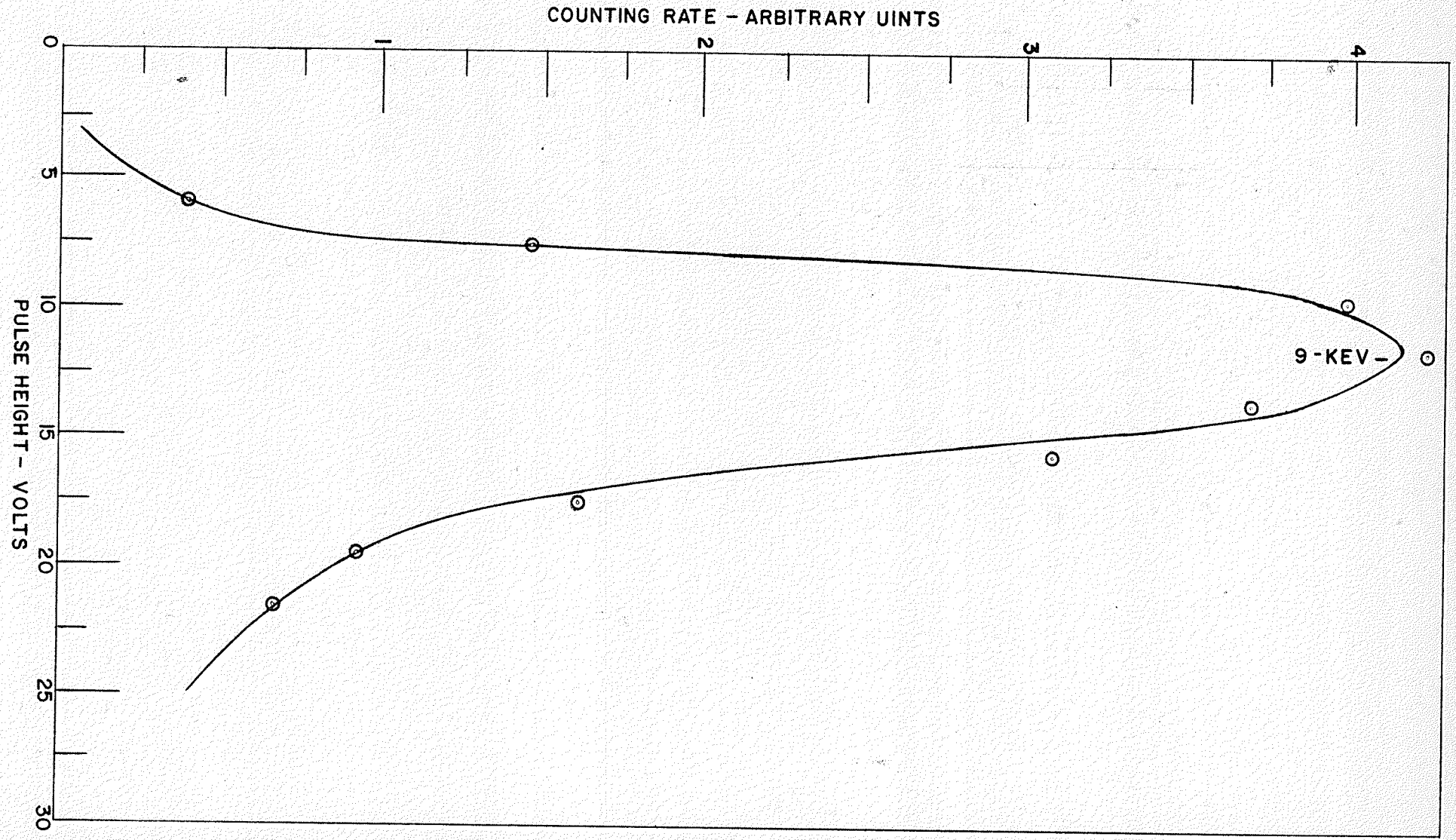
COUNTING RATE – ARBITRARY UINTS
0
1
2
3
4
PULSE HEIGHT – VOLTS
0
5
10
15
20
25
30
9 - KEV

multiplier and filling it with dry ice. Styrofoam, out of which the jacket was made, is a good insulator and easy to work with. With the wall greater than an inch thick it was found that dry ice inside the chamber kept a large fraction of its initial volume for six hours or more. A diagram of the jacket about the photomultiplier appears in figure 2.8. The purpose of the blotting paper is to absorb any moisture that may collect at the base due to the melting dry ice and so prevent it from condensing on the circuitry of the cathode-follower.

(iii) Experimental Results:

The main pulse has been shown to vary linearly with energy over a range 9 kev to 662 kev using various x and gamma rays. Figure 2.9 shows the linear variation from 9 kev to 364 kev.

The pulse height distribution for Rb^{87} was obtained using the small Rb(Tl) crystal as source. The spectrum was analyzed by means of the five channel pulse amplitude analyzer whose first four contiguous channels were varied in width from 0.5 volts to 2 volts to maintain an energy gate of 2.5 kev. Good statistics were obtained by accumulating more than 500 counts at each point. The time required varied from a few minutes to twenty-five hours depending on the energy at which the count was made.

The spectrum from 25 kev on was first obtained using no paralysis in the differentiating circuit. Then with a paralysis of 2.2 msecs. and starting from 11.5 kev the pulse height distribution was determined to the energy where paralysis became ineffective. Figure 2.10 shows the pulse height distribution, corrected for background and paralysis. The curve is composed of three sets of points: a set of points determined with the amplifier at low gain, another with the amplifier at medium gain, and a third set using the maximum gain possible. The three sets of

FIGURE 2.8

PHOTOMULTIPLIER TUBE

REFRIGERATION UNIT

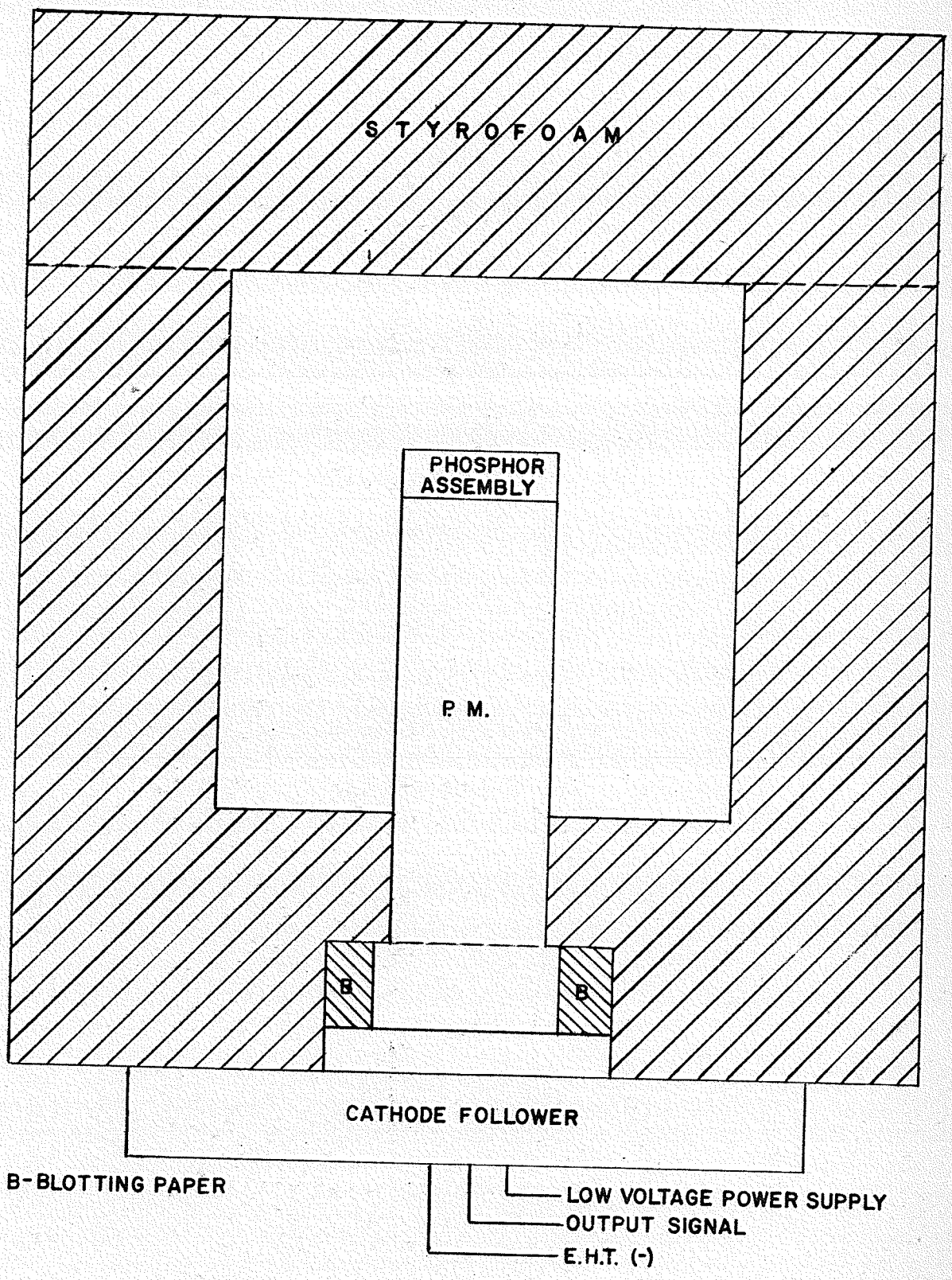
STYROFOAM
PHOSPHOR ASSEMBLY
P. M.
B
B
CATHODE FOLLOWER
B-BLOTTING PAPER
LOW VOLTAGE POWER SUPPLY
OUTPUT SIGNAL
E.H.T. (-)

FIGURE 2.9

LINEAR VARIATION WITH ENERGY

OF PULSE OF RUBIDIUM IODIDE CRYSTAL

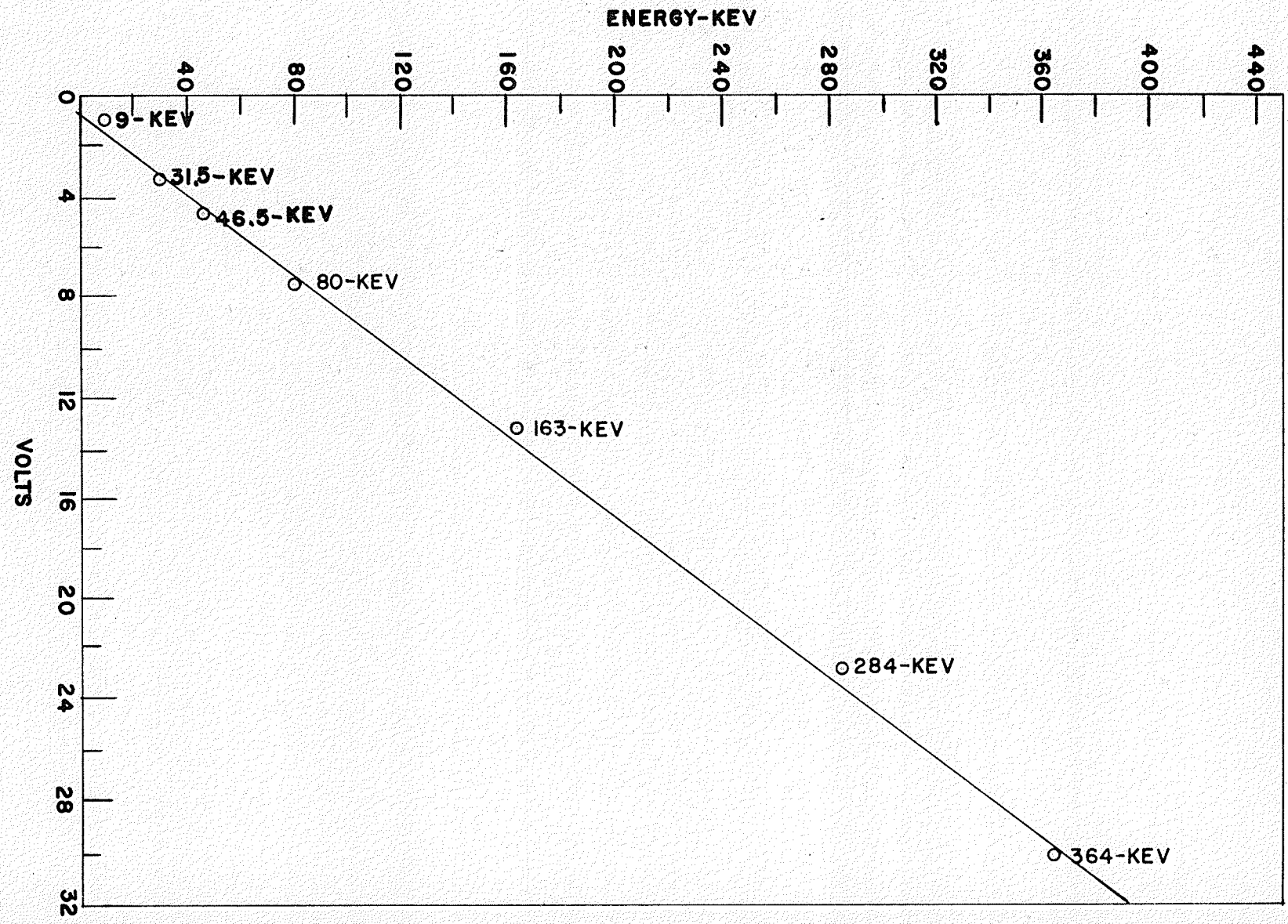
ENERGY-KEV
40
80
120
160
200
240
280
320
360
400
440
VOLTS
0
4
8
12
16
20
24
28
32
9-KEV
31.5-KEV
46.5-KEV
80-KEV
163-KEV
284-KEV
364-KEV

FIGURE 2.10

PULSE HEIGHT DISTRIBUTION SPECTRUM

OF RUBIDIUM 87

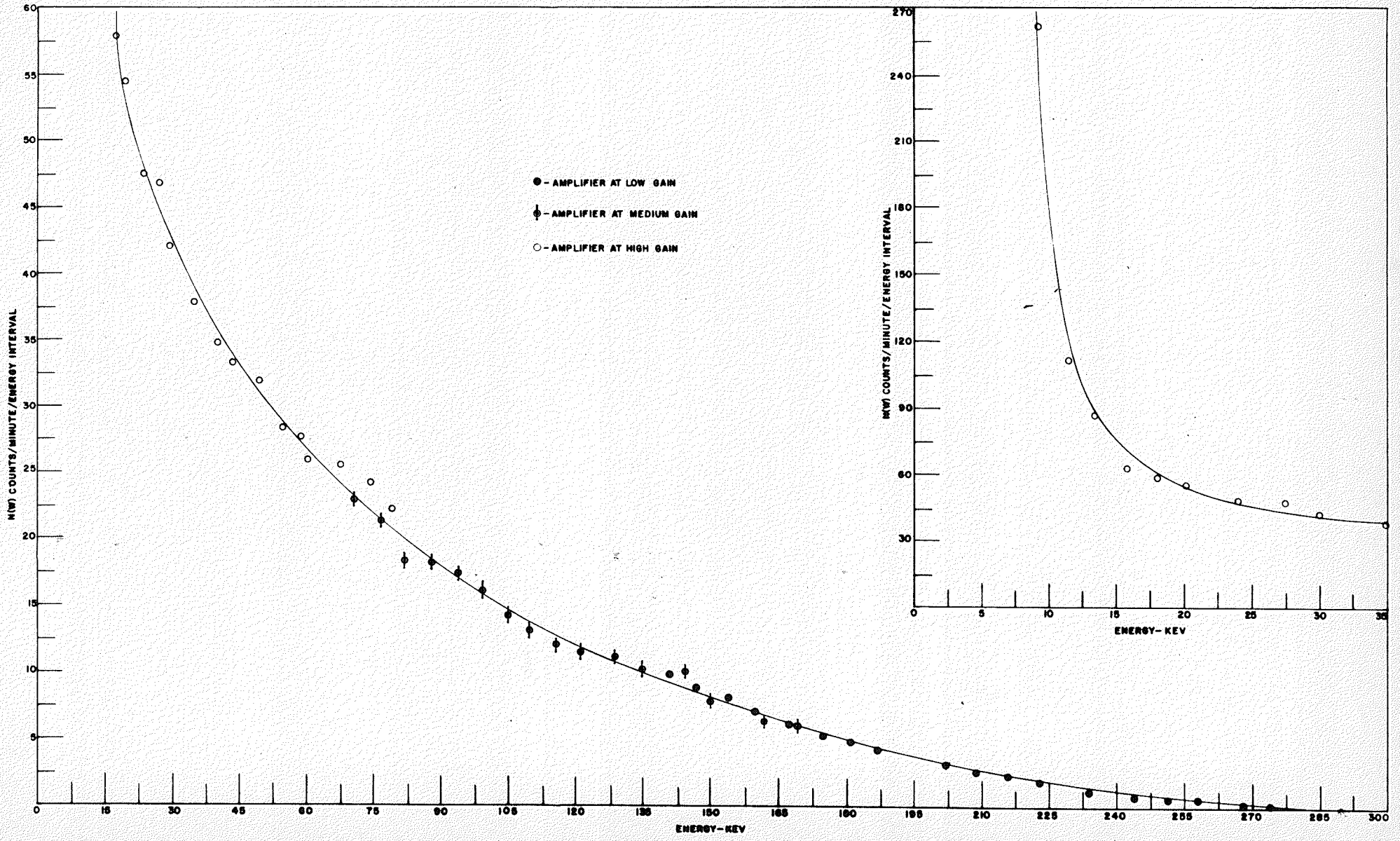
N(W) COUNTS/MINUTE/ENERGY INTERVAL
ENERGY-KEV
⊕ - AMPLIFIER AT LOW GAIN
⊕ - AMPLIFIER AT MEDIUM GAIN
○ - AMPLIFIER AT HIGH GAIN
N(W) COUNTS/MINUTE/ENERGY INTERVAL
ENERGY-KEV

points overlap one another. The deviation of the points from the best line through them is within statistical accuracy. Not all the points obtained are shown in the figure but enough are included to make the drawing of the curve easy. One point below 11.5 kev has been included, namely at 9.25 kev. This was obtained by cooling the photomultiplier tube and crystal to dry ice temperature(-78.5 C). Assuming linearity of pulse height response of the crystal below 9 kev a series of counts in the energy interval between 7.5 and 9.25 kev were made. However, due to the large variation in the values obtained, these have not been included in the plot. Further refinement in technique was terminated when, after the crystal had been cooled and thawed several times, it was discovered to be badly fractured.

To obtain the total counting rate above 11.5 kev, a planimeter was used to find the total area under the curve of the pulse height distribution spectrum given by figure 2.10. The mean of five trials gave 1546 ± 53 counts per minute. Extrapolation to zero energy is required before the total counting rate from the Rb source can be determined.

(iv) Determination of Half-life:

Due to the rapid rise in the pulse height distribution in the low energy region, direct extrapolation of the raw spectrum to zero energy is not feasible. Instead the extrapolations were carried out on the allowed Fermi plot of the Rb^{87} beta-spectrum. For the purpose of computation equation 1-11 was rewritten as:

$$\left[\frac{N(W)dW}{W^2G}\right]^{1/2} \propto (W_o - W) \qquad (2.1)$$

where $G = pF/W$.

Values of the modified Fermi function G as a function of p, the electron momentum, were taken from the tabulation by Rose(45). The values for Z=38 and A=90 were chosen; and values of G at intermediate values of p were obtained by interpolation. Figure 2.11 shows the curve for $\left[N(W)/W^2G\right]^{1/2}$ vs. energy W. Although the raw spectrum of Rb^{87} indicates an end-point energy of 275 kev the allowed Fermi plot does not. Linear extrapolation to zero counting rate from the last seven points of the plot indicates an end-point energy of 294 kev. Langer et al(48) have pointed out that the conventional Fermi plot must be corrected for the finite resolution of the spectrometer. The effect of the resolution on the shape of the spectrum is particularly evident near the end-point. Applying the resolution corrections of Palmer and Laslett(49) to the second forbidden Cl^{36} beta-spectrum, Langer et al found the corrections to be 2% or less at each point except for the five points nearest the end point. Applying a resolution correction to the points near the end-point energy causes these points to have a lower ordinate value. In view of these facts it is suggested that the allowed Fermi plot of the experimentally obtained Rb^{87} beta-spectrum has an end-point energy somewhat less than 294 kev. An end-point energy of 275 kev is therefore used in subsequent calculations, this being the mean of several values*. It is also noteworthy that since the effect of making a resolution correction for the points at the low energy end is small, the linear extrapolation of the Fermi plot from 10 kev to zero energy, as carried out in figure 2.11, appears reasonable. From this extrapolation an additional 383 counts per minute were obtained, yielding a total counting rate of 1929±65 counts per minute. The estimated error of 65 counts per minute is the error due to the standard deviation in the integral count above 11.5 kev.

* The mean end-point energy of 275 kev was obtained by averaging the values given by Lewis(23), MacGregor and Wiedenbeck(21), and Curren et al(20) with the one obtained in this experiment.

FIGURE 2.11

ALLOWED FERMI PLOT

OF

RUBIDIUM 87 BETA-SPECTRUM

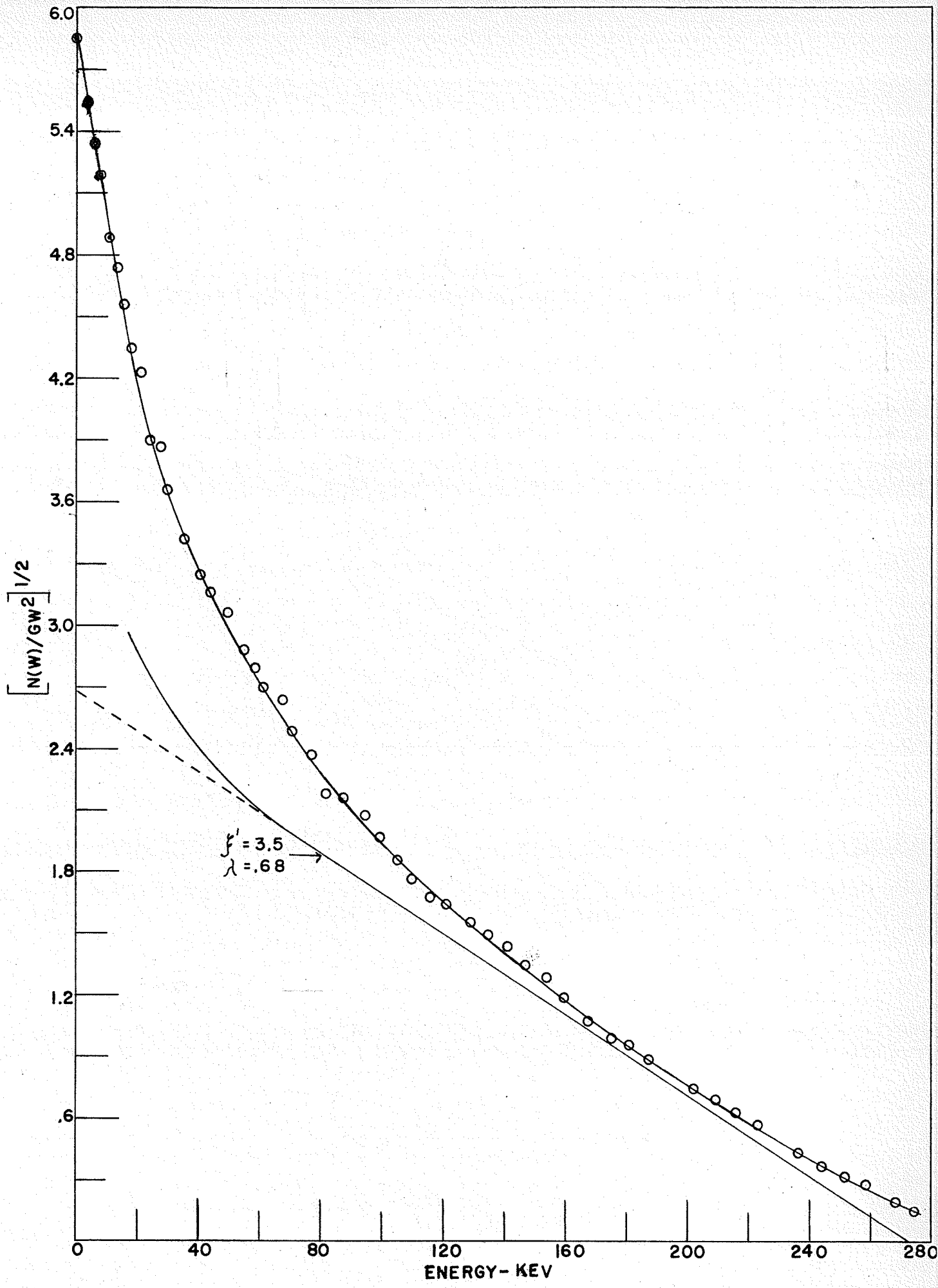
6.0
5.4
4.8
4.2
3.6
3.0
2.4
1.8
1.2
.6
[N(W)/GW²] 1/2
0
40
80
120
160
200
240
280
ENERGY - KEV
ξ' = 3.5
λ = .68

With a RbI(Tl) source of 0.0938 ± .00005 gms. and a 27.85% abundance of the isotope Rb^{87}, the specific activity of the beta-decay process works out to 855.5 disintegrations per second per gram of rubidium, corresponding to a half-life of $(5.04 \pm .2) \times 10^{10}$ years, which agrees with the calculated value of the half-life of Rb^{87} as given by Witherill et al(47). It is not in agreement with the currently accepted half-life of 6.2×10^{10} years, and in particular, is not in agreement with Lewis' value of $(5.9 \pm .3) \times 10^{10}$ years. Comparison of the total counts above 17.5 kev indicates agreement well within statistical accuracy. It is therefore, suggested that the additional counts obtained by Lewis in extrapolating to zero energy are too conservative.

(v) Theoretical Interpretation:

With $\log_{10} f(Z,W_o)$ equal to -0.68 for an end-point energy of 275 kev (14) a value of 17.52 is obtained for the comparative half-life, $\log_{10} f(Z,W_o)\, t$, and the transition $Rb^{87} \rightarrow Sr^{87}$ is third forbidden. The nuclear spin change of 3(yes) between the ground states $p_{3/2} \rightarrow g_{9/2}$ accords with this. A theoretical correction factor to the Fermi plot shape has been formulated by E. Konopinski(9), and has been given in equation 1.9 . For a third forbidden spectrum this may be re-written after dividing by $\Sigma \left| \int \beta \psi_{nm} (\underline{\sigma} \times \underline{r}) \right|^2 / C_T^2$ as:

$$S_3(W) \propto C \left\{ P_3(\underline{\sigma} \times \underline{r}) + \lambda^2 (\alpha Z/2\rho)^2 P_3(\underline{\alpha}) + (\xi')^2 P_3(\underline{r}) + \lambda(\alpha Z/\rho) I_3(\underline{\sigma} \times \underline{r}, \underline{\alpha}) + 2(\xi') I_3(\underline{\sigma} \times \underline{r}, \underline{r}) + \lambda(\alpha Z/\rho)(\xi') I_3(\underline{\alpha}, \underline{r}) \right\} \qquad -- 2.2$$

where $\xi' = \frac{C_S}{C_T} \xi$, and $\left(\frac{\alpha Z}{\rho}\right) = 17.3\ mc^2$. λ and ξ' are variable parameters with which the allowed Fermi plot is to be linearized. λ and ξ were defined by equations 1.10 . ξ is readily calculated either by using the single particle shell model or the special j-j coupling shell model in which outer neutrons and protons enter into the same shells,

respectively(24). In the latter case only the angular part of the wave function is required since the radial part drops out as a common factor. Yamada et al(24) give $\xi = -1$ for Rb^{87} and state that the sign of C_S/C_T is probably minus. It is therefore expected that ξ' should be positive. The ratio, λ, on the other hand, cannot be calculated as reliably. Yamada(50), defining λ by $\lambda\left(\frac{2Z}{2\rho}\right) = n \frac{Q_n(\beta\alpha, \underline{r})}{Q_n(\beta \underline{\sigma} \times \underline{r}, \underline{r})}$

obtains for $\lambda\left(\frac{2Z}{2\rho}\right)$ a value of 7.12 for Rb^{87}. With the Coulomb energy of the daughter nucleus $(\alpha Z/\rho)=17.3\ mc^2$, λ becomes .823 .

In determining what values to use for the two parameters an experimental shape factor is obtained as

$$S_3(exp) = N(W)/GW^2(W_o-W)^2 \qquad \text{---- (2.3)}$$

by putting the experimental values of N(W) into equation 1.7 . Figure 2.12 shows the Rb^{87} experimental shape factor for two end-point energies, 275 kev(1.538 mc^2) and 294 kev(1.575 mc^2). Clearly, $S_3(exp)$ becomes very sensitive to the value adopted for the end-point energy, W_o, for the energies near W_o. Subsequent calculations were made on the basis of an end-point energy of 275 kev.*

In fitting the "exact" shape factor $S_3(W)$, equation 2.2, to the experimental data, $S_3(exp)$, values of ξ' from -7 to +31 were tried. For each trial of ξ', λ was determined by solving equation 2.2 with the quantity on the left set to $S_3(exp)$ for 20 kev. Both roots of the quadratic equation in λ were tried in $S_3(W)$ for other energies. The results of some of the calculations are shown graphically in figures 2.12 and 2.13 . The best agreement between $S_3(exp)$ and the theoretical shape factor was found for $\xi'=3.5$, $\lambda=.68$ and $\xi'=25$, $\lambda=4.59$. The allowed Fermi plots of Rb^{87}, linearized by the resulting two shape factors, are shown in Figures 2.11 and 2.13, respectively. The Fermi plot is linearized except at the low energy end. This non-linearity at the low energy end

* See footnote on Page 35.

FIGURE 2.12

EXPERIMENTAL AND THEORETICAL

SHAPE CORRECTION CURVES

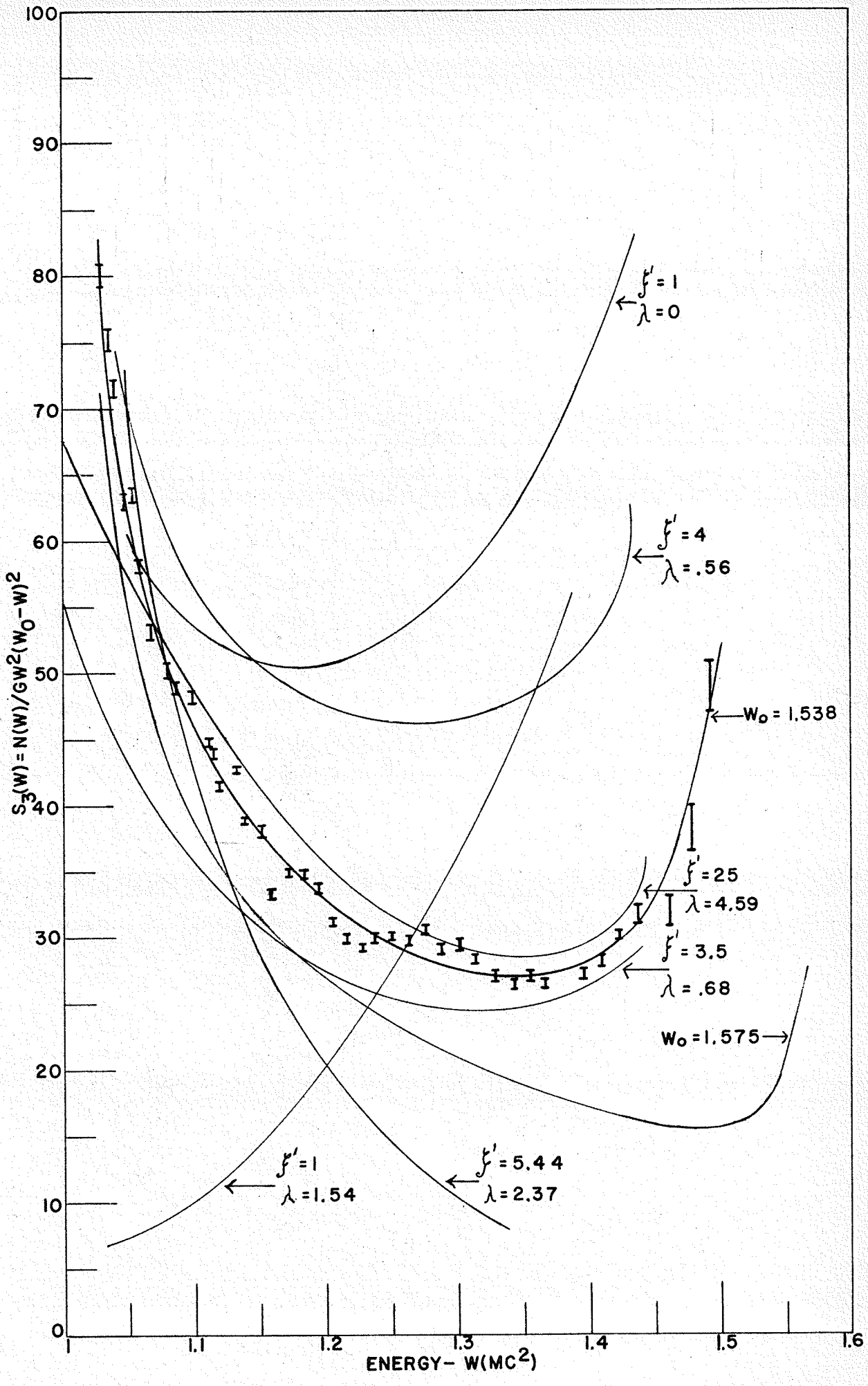
100
90
80
70
60
50
40
30
20
10
0
1
1.1
1.2
1.3
1.4
1.5
1.6
$S_3(W) = N(W)/GW^2(W_0-W)^2$
ENERGY- $W(MC^2)$
$\xi' = 1$
$\lambda = 0$
$\xi' = 4$
$\lambda = .56$
$W_0 = 1.538$
$\xi' = 25$
$\lambda = 4.59$
$\xi' = 3.5$
$\lambda = .68$
$W_0 = 1.575$
$\xi' = 1$
$\lambda = 1.54$
$\xi' = 5.44$
$\lambda = 2.37$

FIGURE 2.13

ALLOWED FERMI PLOT OF Rb^{87}

CORRECTED WITH THEORETICAL

SHAPE FACTOR

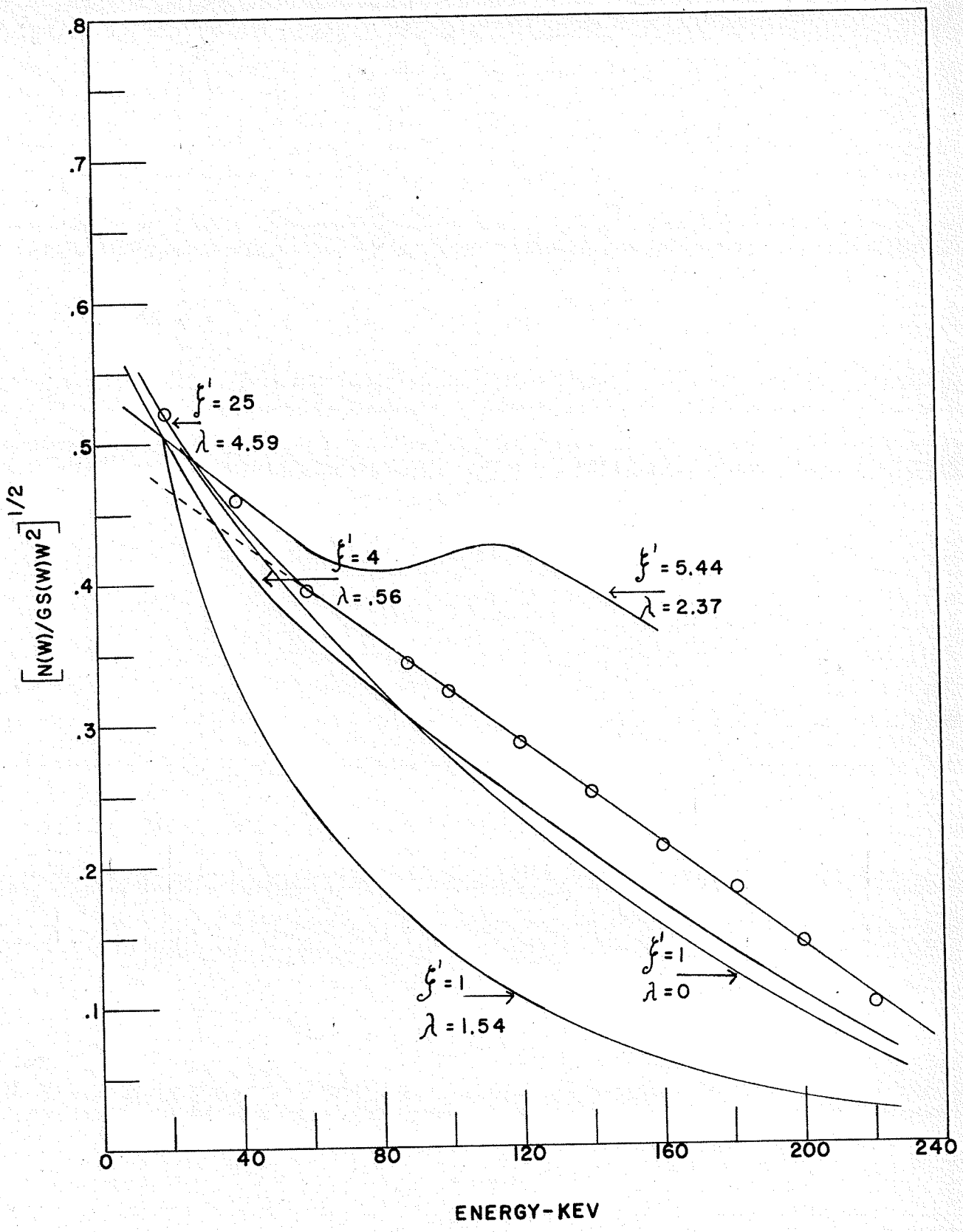
.8
.7
.6
.5
.4
.3
.2
.1
0
40
80
120
160
200
240
[N(W)/GS(W)W²]^1/2
ENERGY-KEV
ξ' = 25
λ = 4.59
ξ' = 4
λ = .56
ξ' = 5.44
λ = 2.37
ξ' = 1
λ = 0
ξ' = 1
λ = 1.54

is in part due to what might be termed, the edge effect, which is simply that an undetermined number of beta-particles emitted from the Rb^{87} nucleus near the surface of the RbI(Tl) crystal escape from the crystal without expending any considerable portion of their kinetic energy. Libby(51) gives, for the maximum range of the beta-particle from Rb^{87}, a value of 20 mg/cm^2. For normal incidence electrons will then escape without losing any, or only some, of their kinetic energy from a surface layer thickness of 5.64×10^{-3}cms. Due to the very small crystal used the volume of this surface layer, assuming a cubic crystal, represents 7.56% of the total volume of the crystal. However, it is expected that at least half of the beta-particles emitted within this critical volume are emitted with initial directions into the crystal and that therefore, it is perhaps reasonable to assume that only about 3-4% of the total crystal volume is ineffective in totally absorbing the beta-particles emitted. The fact that most of the counts occur at the low energy end of the distribution spectrum suggests that this edge-effect may be of smaller magnitude than indicated. Calculations show that a correction of this magnitude does not linearize the shape corrected Fermi plot at the low energy end.

Since ξ' is much greater than zero it is implied that pure tensor interaction does not explain the Rb^{87} plot. The present "best" value of $(C_S/C_T)^2$ has been given in the foregoing, equation 1.13 . Written as an inequality it is:

$$0.29 \leq (C_S/C_T)^2 \leq 1.04$$

The ratio ξ may then be calculated from $\xi' = (C_S/C_T)\,\xi$. Values of the ratios of the three nuclear matrix elements involved in the correction factor required to analyze the third forbidden Rb^{87} beta-spectrum are given in the following table:

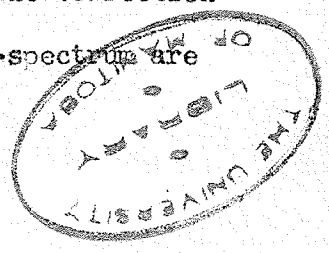

TABLE 2.1

RATIOS OF NUCLEAR MATRIX ELEMENTS INVOLVED

IN Rb^{87} SPECTRUM CORRECTION FACTOR

λ	$\frac{\int(\beta)\,\mathcal{Y}_{nm}(\underline{\alpha})}{\int(\beta)\,\mathcal{Y}_{nm}(\underline{\alpha}\times\underline{r})}$	ξ'	$(C_S/C_T)^2$	$\xi = i\frac{\int(\beta)\,\mathcal{Y}_{nm}(\underline{r})}{\int(\beta)\,\mathcal{Y}_{nm}(\underline{\alpha}\times\underline{r})}$
.68	5.88	3.5	$.29 \leq (C_S/C_T)^2 \leq 1.04$	$3.42 \leq \lvert\xi\rvert \leq 6.5$
4.59	39.7	25	$.29 \leq (C_S/C_T)^2 \leq 1.04$	$24.5 \leq \lvert\xi\rvert \leq 46.5$

The value of .68 for λ in the first instance, compares favourably with Yamada's theoretical value of .823. The value of -1 for ξ, calculated theoretically by Yamada et al(24) on the basis of the single particle shell model does not fall within the experimental range as given by $3.42 \leq |\xi| \leq 6.5$. In the second instance the large values of 4.59 and 25 for λ and ξ', respectively, result in making the radiation term $P_3(\underline{\alpha} \times \underline{r})$ in equation 2.2 negligible. No theoretical justification for doing so exists. The resulting shape factor, however, appears equally effective in linearizing the Rb^{87} beta-spectrum.

Chapter III

VANADIUM 50

(i) Introduction:

Leland(12) has reported the natural occurrence of an isotope of vanadium of mass 50 and an abundance of $0.23 \pm .01\%$ as measured by a mass spectrometer. Johnson(44) has measured the mass differences between V^{50}, Ti^{50} and Cr^{50}. He has found that V^{50} is more massive than Ti^{50} and Cr^{50} by 2.39 ± 0.12 Mev and $1.18 \pm .12$ Mev respectively. Ample energy is therefore available for decay of V^{50} to Cr^{50} or Ti^{50} to occur. Failure to detect this activity is attributed to a long half-life.

The nuclear spin of V^{50} has been measured to be 6(43). This agrees with the results of theoretical calculations based on the shell model. According to the nuclear shell model V^{50} ($N = 27$, $Z = 23$) has 7 neutrons and 3 protons in $f_{7/2}$ orbitals and hence has even parity in the ground state. The neighboring isobars Ti^{50} ($N = 28$, $Z = 22$) and Cr^{50} ($N = 26$, $Z = 24$) are even-even nuclei and are therefore expected to have ground state spins $J = 0$ and even parity. The ground-ground state transitions from V^{50} to Ti^{50} or Cr^{50} are therefore expected to be "sixth forbidden." The associated half-lives for these transitions may therefore be expected to be very long.

The first excited level of Ti^{50} has been determined to be $1.58 \pm .06$ Mev(37) and according to the systematics on even-even nuclei(33), it is expected to have a spin $J = 2$ and even parity. With $\Delta J = 4$ and no parity change, the K capture transition between the ground state of V^{50} and the first excited level of Ti^{50} can be classified as "fourth forbidden." A

rough estimate of the half-life can be obtained by considering the comparative half-lives for beta transitions of this order. If log ft = 23 is taken as being characteristic of fourth forbidden transitions and log f for a K capture transition in V^{50} for a decay energy of 0.81 Mev is taken from curves given by Feenberg(14) and Trigg, then a value of 9.6×10^{15} years is obtained for the half-life.

The presence of a measurable negatron activity proceeding to an excited level of Cr^{50} is unlikely. Goldhaber's(33) plot of the energies of the first excited levels of even-even nuclei against the number of neutrons shows that the energy of the first excited level of even-even nuclei varies smoothly and decreases, in general, with increasing mass number. It is, therefore, expected that the first excited level of Cr^{50} should be approximately the same as that for Ti^{50}. Goldhaber also points out that in a large number of examples, the addition of two protons to a nucleus hardly affects the energy of the first excited level. Ti^{48}(N = 26, Z = 22) is known to have a first excited level at 1.35 Mev. It is, therefore, expected that the first excited level of Cr^{50} is at least of the order of the V^{50} - Cr^{50} mass difference. It then follows that the energy available for such a transition is so low as to make the associated half-life too long to measure.

Numerous attempts(30,31,32,27) to detect the long-lived radioactivity of the V^{50} isotope have been made in the past. The literature up to the near present has been fully reviewed recently(27) and will, therefore, not be attempted here. In this recent attempt a search for the 1.58 Mev gamma ray was made using a scintillation spectrometer, which was housed in the massive shield shown diagrammatically in figure 2.3. Using a 1 1/4 x 1 1/2 inch NaI(Tl) crystal mounted in an aluminum can a compara-

tively large background counting rate of 1.13 ± 0.02 counts per minute was obtained in the energy interval between 1.45-1.70 Mev. For the source 200 grams of vanadium metal turnings (99.9% pure) were used. A mean sample plus background counting rate of 1.16 ± .02 counts per minute was obtained in the same energy interval, leaving a net activity of 0.03 ± 01 counts per minute for the 1.58 Mev gamma radiation.

No attempt was made to determine to what extent the presence of the source distorted the background counting rate. With the net activity being of such dubious magnitude this ommission becomes important. Furthermore, although, preliminary work revealed the presence of low energy gamma radiation, indicating that the vanadium sample was contaminated with some radioactive impurities, no attempt to identify, qualitatively or quantitatively, the impurity was made. The small net activity observed cannot, in the light of these ommissions, be regarded as being wholly due to the 1.58 Mev gamma radiation.

In considering the possibility of reducing the overall background counting rate cognizance must be taken of the fact that the presence of radioactive impurities in the materials of the NaI(Tl) crystal-photomultiplier combination sets a lower limit on the background. The presence of trace amounts of potassium in the glass of the photomultiplier cannot easily be eliminated. DuMont is looking into the possibility of producing radioactive free photomultipliers and special low background tubes should be available in the near future(34). What is perhaps more easily eliminated are the impurities in the crystal assembly. An analysis of the sources of background in NaI counting has been made by C.E. Miller of Argonne National Laboratory(35). He has shown that a large fraction of the residual background counting rate was due to radiation from the radium

in the aluminum in which the NaI crystals are usually mounted. It was found that samples of Al, regardless of alloy type or supplier, averaged 0.3 uuc of Ra per gram of Al. Mounting the crystal in a No. 304 stainless steel can reduced the background by 60% in the 0.090 - 2.15 Mev region of the spectrum. No beta or gamma activity was found to be attributable to the MgO reflector or the Tl activator.

In view of these recent advances in technical knowledge it was felt that another attempt at detecting the radioactivity of V^{50} should be undertaken. The following is a brief account of the techniques employed and the results obtained.

(ii) Apparatus:

Three sheets of stainless steel (No. 304) and one sheet of electrolytic copper were tested for radioactive contamination by counting in the 1 - 2 Mev interval using samples of these sheets as source, and subtracting the background counting rate in each case. Of the three sheets of stainless steel only one was found to be uncontaminated. By using a 1 1/4 x 1 1/2 inch Al canned NaI(Tl) crystal, the sample plus background, and background, counting rates for this particle were found to be 15.82±0.1 and 15.80±0.3 counts per minute, respectively. The net activity of 0.02 counts per minute is within the statistical error. Similarly, the sample plus background, and background, counting rates for the copper sheet were determined to be 15.45 ± .12 and 16.12 ± .29 counts per minute in the same energy interval. The deficit of 0.67 counts per minute is greater than the standard deviation and it may therefore be presumed that this sample of electrolytic copper was free from radioactive impurities. In view of the fact that there was no local spinner able to use the 26 gauge No: 304 stainless steel in spinning a proper container for an unmounted 1 1/4 x 1 1/2

inch NaI(Tl) crystal, the copper sheet was used instead, it being only five and one-half thousandths of an inch thick. The crystal was obtained from the Harshaw Chemical Company and mounted locally at Nuclear Enterprises Limited in a manner shown diagrammatically in figure 3.1 and described by P.R. Bell(36). A three inch lucite light piper was used in place of a glass window for two reasons, namely, that it removes the crystal from the contaminated glass of the photomultiplier and eliminates the use of potassium-containing glass for the window.

To accomodate the use of a light piper a ten inch extension of the lead shield shown diagrammatically in figure 2.3 had to be made. With this in place several lengths of lucite light pipe were tried, simply by adding four inches at a time to the three inches already incorporated into the phosphor assembly. The variation in the resolution and pulse height of the 662 kev gamma from Cs^{137} for the same overall gain is shown in the following table:

TABLE 3.1

PULSE HEIGHT AND RESOLUTION

Type of Photomultiplier	Length of Pipe	Pulse Height	Resolution
K1190(1 inch)	7 inches	12.5 Volts	60%
K1190	3 inches	16 Volts	47%
K1190	0 inches	21 Volts	14.3%
352 (2 inch)K1186	0 inches	25 Volts	14%

An analysis of the background counting rate using the various lengths of light pipe and the different photomultipliers is shown graphically in figure 3.2. The difference in the background obtained by using

FIGURE 3.1

PHOSPHOR ASSEMBLY

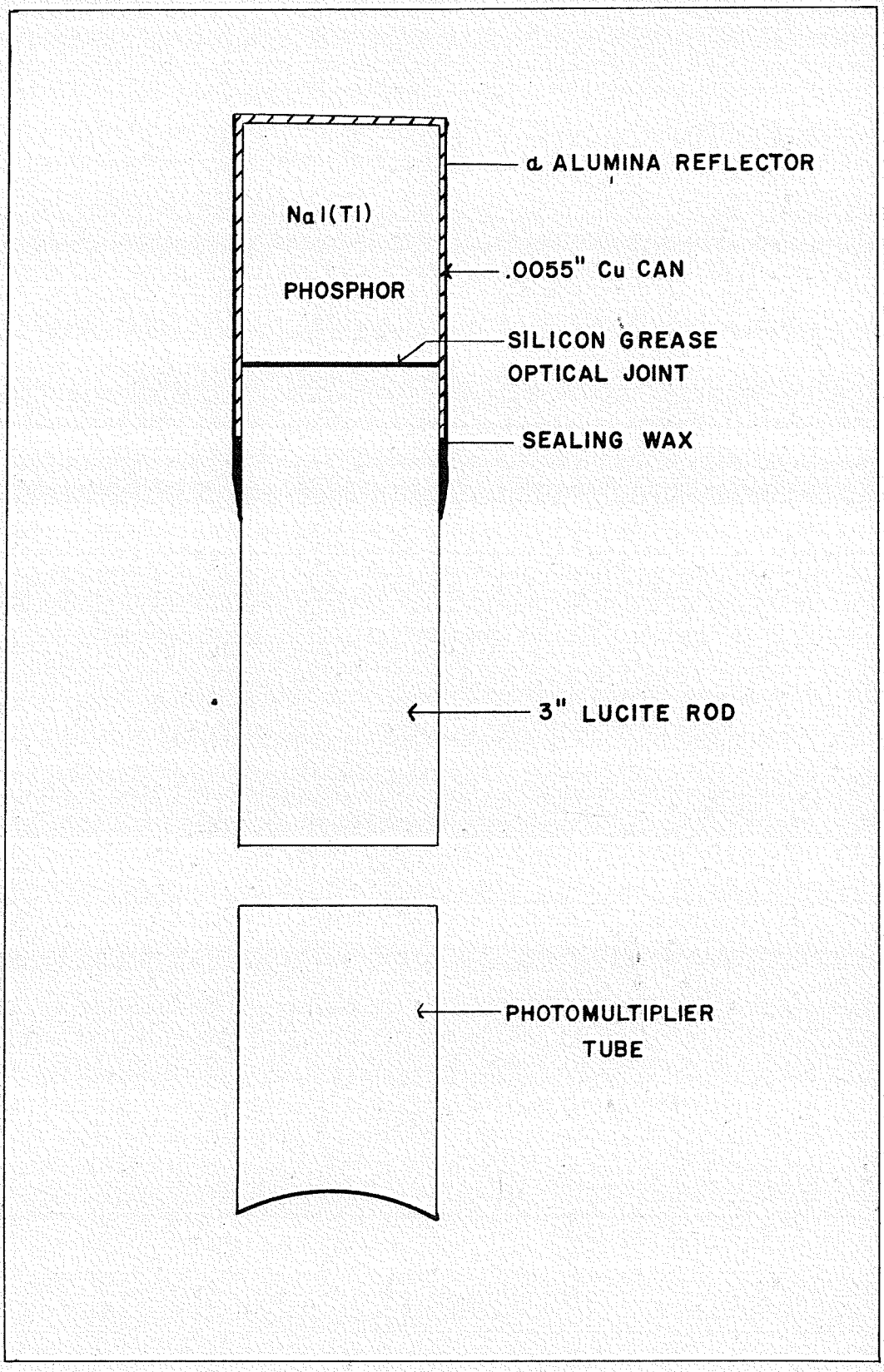
α ALUMINA REFLECTOR
NaI(Tl)
PHOSPHOR
.0055" Cu CAN
SILICON GREASE
OPTICAL JOINT
SEALING WAX
3" LUCITE ROD
PHOTOMULTIPLIER
TUBE

FIGURE 3.2

BACKGROUND ANALYSIS

WITH

PHOSPHOR ASSEMBLY

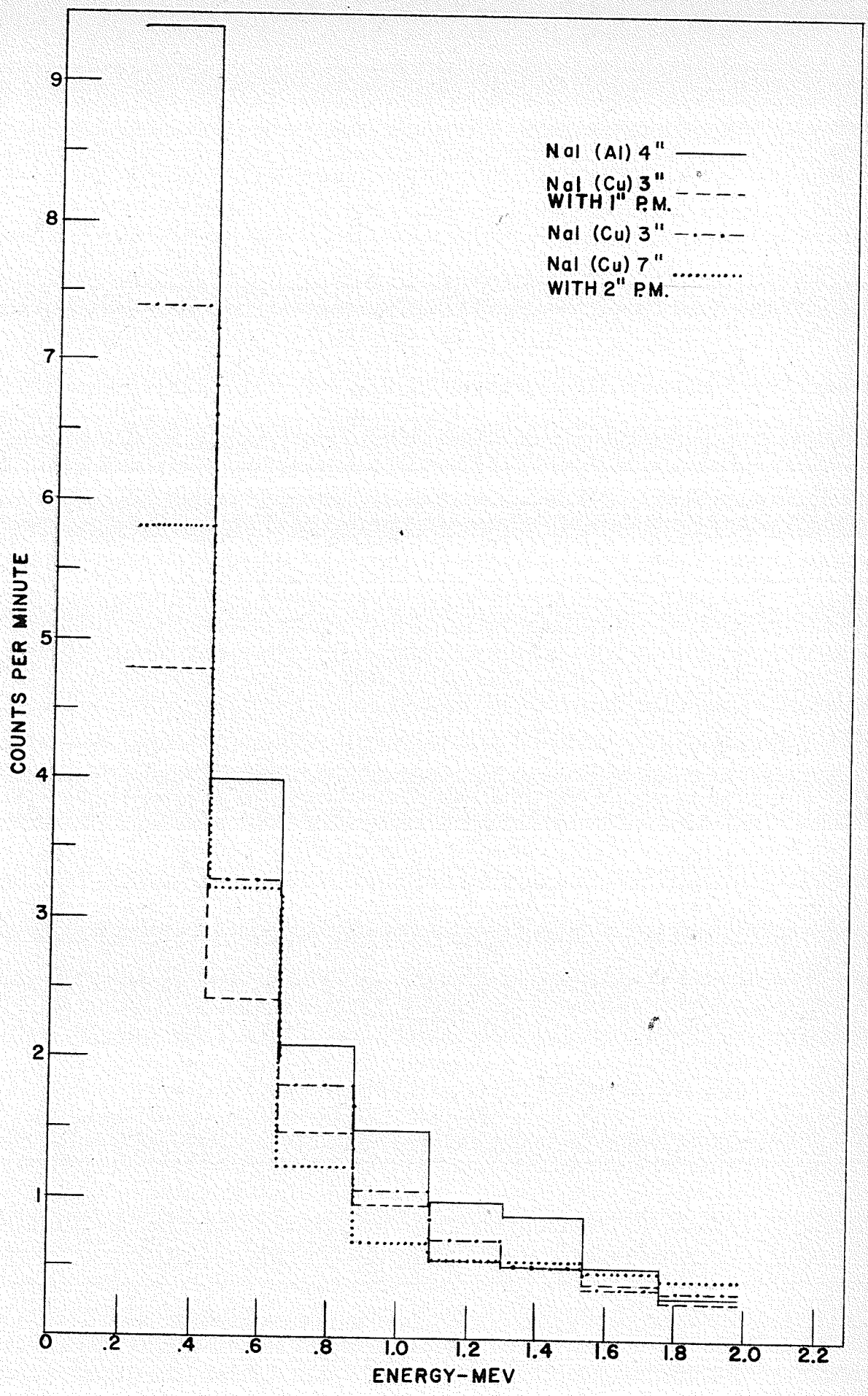
NaI (Al) 4"
NaI (Cu) 3" WITH 1" P.M.
NaI (Cu) 3"
NaI (Cu) 7" WITH 2" P.M.
COUNTS PER MINUTE
ENERGY-MEV
0
.2
.4
.6
.8
1.0
1.2
1.4
1.6
1.8
2.0
2.2
1
2
3
4
5
6
7
8
9

an aluminum canned NaI crystal (NaI(Al)) and a copper canned NaI crystal (NaI(Cu)) is relatively large. The reduction in the background counting rate in the .45 - .67 and 1.55 - 1.77 Mev intervals is 17.5% and 27% respectively. Compare the solid line with the dash-dot line of figure 3.2. Both of these, as well as the dotted line, which corresponds to a seven inch light pipe, were obtained with the two-inch photomultiplier.

The dashed line shows the histogram obtained when the one-inch photomultiplier was used in combination with the phosphor assembly shown in figure 3.1. The background reduction is largest in the low energy region of the spectrum. Nevertheless, the background reductions realized in 100 kev gates in the 1.50 and 1.60 Mev regions by using the one-inch photomultiplier with the phosphor assembly amount to about 40% and 25% respectively. In view of this significant reduction in the background counting rate and with the resolution of the two tubes being about the same, the one-inch photomultiplier was used in the subsequent experiment. The pulse height distribution was obtained by the apparatus already described in Chapter II.

For the source 186 grams of vanadium metal turnings (99.9% pure) were packed into a paper container fitted snugly over the crystal so that it covered the crystal on all free sides to a thickness of about 0.3 inches of vanadium. This was the source used in an earlier experiment(27) and was found to contain a radioactive impurity. Corrections, allowing for this impurity are described and calculated in the subsequent section.

(iii) Experimental Procedure and Results:

An attempt was made to detect the predicted K capture activity in V^{50} by measuring the 1.58 Mev photoline counting rate from the vanadium sample and comparing it with the photoline counting rate for gamma rays

of 1.465 Mev coming from 71.6 grams of KCl in the same geometry. Calibration of the energy scale was carried out with the photolines from Cs^{137} (0.662 Mev) and Co^{60} (1.17, 1.33 Mev). Knowing the variation of spectrometer resolution with gamma ray energy the gate required to include all the activity of the photoline from the predicted 1.58 Mev gamma ray was calculated. The four contiguous channels of the pulse amplitude analyzer were then adjusted in width so as to include just this gate. Background and sample counts were alternated every eight hours, this practice being largely a precaution against serious drift. The results of the series of runs are tabulated below:

TABLE 3.2

VANADIUM SAMPLE ACTIVITY

Background	gate 1.46-1.74 Mev		Vanadium (186 grams)		
Time (mins.)	Counts	Ctg. Rate (cpm)	Time (mins.)	Counts	Ctg. Rate (cpm)
240	157	0.65 ± .05	405	279	0.69 ± .04
385	198	0.51 ± .03	420	196	0.46 ± .03
390	182	0.46 ± .03	560	350	0.63 ± .03
460	206	0.45 ± .03	585	396	0.67 ± .03
475	218	0.46 ± .03	915	585	0.64 ± .02
1950	961	0.49 ± .015	2885	1806	0.62 ± .014

Net counting rate due to vanadium sample = 0.13 ± .02 cpm. A histogram of the net activity possibly due to a 1.58 Mev gamma is given in figure 3.3. The presence of the 1.58 Mev gamma ray is indicated.

The counting rate in the 1.465 Mev photoline of K^{40} from the KCl

FIGURE 3.3

HISTOGRAM OF PREDICTED

1.58 MEV GAMMA RAY

FROM VANADIUM 50

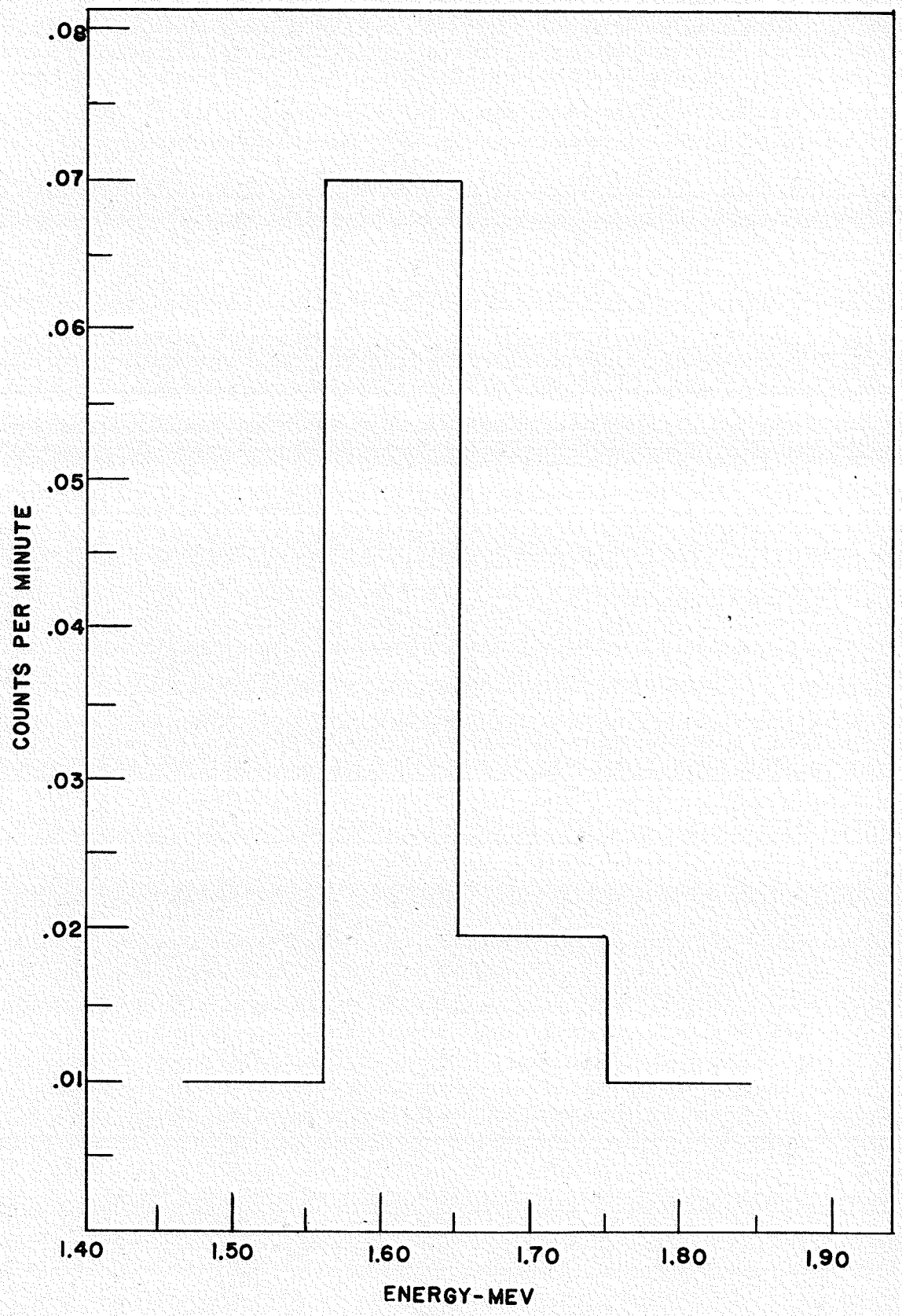
.08
.07
.06
.05
.04
.03
.02
.01
COUNTS PER MINUTE
1.40
1.50
1.60
1.70
1.80
1.90
ENERGY-MEV

sample in the same geometry was measured with the lower and upper channel levels set to pass pulses whose energies were between 1.33 and 1.60 Mev. The results are tabulated below:

TABLE 3.3

K^{40} ACTIVITY

Background	gate (1.33-1.60 Mev)		KCl (71.6 grams)		
Time (mins.)	Counts	Ctg. Rate (cpm)	Time (mins.)	Counts	Ctg. Rate (cpm)
385	198	$0.51 \pm .03$	180	10505	$58.36 \pm .5$
240	157	$0.65 \pm .05$	180	11611	$64.50 \pm .6$
625	357	$0.56 \pm .03$	360	22116	$61.43 \pm .4$

Net counting rate due to 71.6 grams of KCl = $60.87 \pm .5$ cpm.

To determine the background enhancement factor, that is, the extent by which the presence of the source distorts the background counting rate by its interaction with the background radiation, chromium metal (fused) in the form of granules was placed in a paper container similar to the one used for the vanadium source. A count of the background with and without the chromium sample revealed that a net counting rate of $0.26 \pm .03$ counts per minute could be attributed to the chromium sample. Of the three possible types of interaction of gamma rays with matter the Compton effect becomes predominant at medium energies (the partial absorption coefficients of the photoelectric effect, the Compton effect, and of pair production are proportional to ρZ^5, ρZ, ρZ^2 respectively) and it might therefore be expected that the observed net activity for the vanadium and chromium samples in the 1.46 - 1.74 Mev energy interval could be due to Compton

processes resulting from the interaction of medium energy gamma radiation from radioactive contamination in the Pb shield, photomultiplier tube, or from the interaction of cosmic rays with the samples. Regardless of what type of interaction it actually is,* the ratio of the net counting rate due to the vanadium sample to that due to the chromium sample should be about 0.83 since the Z numbers of the two samples differ only by one unit and 0.83 is the ratio of their densities. The observed ratio is $0.5 \pm .14$. Therefore, the possibility that the observed net activity for the vanadium and chromium is wholly due to the interaction of the background radiation with the samples, seems unlikely. This suggests that the chromium metal was also contaminated, in which case the background enhancement factor as given above is not a reliable estimate and cannot legitimately be used to correct the observed activity of the vanadium sample in the 1.46 - 1.74 Mev energy interval for background distortion. The counting rate of $0.13 \pm .02$ counts per minute can, in the light of the foregoing, be regarded as representing an upper limit to the activity of the vanadium sample in the 1.46 - 1.74 Mev energy range.

An attempt was made to correct the vanadium sample counting rate in the 1.46 - 1.74 Mev interval for the activity of the contaminant referred to earlier. Since the principal vanadium ores are(38): carnotite (potassium uranyl vanadate) $2U_2O_3.V_2O_5.K_2O\ 3H_2O$, patronite, an impure vanadium sulfide, and vanadinite $Pb_5(VO_4)Cl_3$, the possibility of the contaminant being any of the products of the Thorium or (and) Uranium decay series suggests itself. The three series may be differentiated by the fact that one of the products of the Thorium series, $_{81}Tl^{208}$ emits an intense gamma of energy 2.62 Mev while the highest energy gamma from any of the products of the Uranium series is the relatively weak 2.42 Mev

* It was found that the counting rate of the radiation from Co^{60} in the 1.2-1.4 Mev interval was reduced on the average by 5% when the vanadium sample was interposed between the source and the crystal. Therefore the interaction of the background radiation with the sample is small.

emitted by $_{83}Bi^{214}$ as it decays to $_{84}Po^{214}$(28)(39). It was decided therefore, to determine the contribution to the vanadium sample counting rate of 0.13 counts per minute of a possible thorium or (and) uranium family contaminant. The thorium contribution was determined by measuring the counting rate of the vanadium sample and a thorium sample in the 1.46 - 1.74 Mev and 2.56 - 2.66 Mev intervals. The results are tabulated below:

TABLE 3.4

Source	Counting rate: in 1.46 - 1.74 Mev	In 2.56 - 2.66 Mev
Vanadium	0.13 ± .02 cpm	c = .007 ± .016 cpm
Thorium	a = 4908 cpm	b = 1447 cpm

The quantity (ac/b) = .024 counts per minute gives some measure of the contribution of a possible thorium contaminant. Similarly in considering the possibility of the contaminant being of the uranium series an upper energy interval was chosen between 1.70 - 1.88 Mev, this being the region where the pulse height distribution spectrum of a Uranium sample exhibits an intense line. This energy interval includes some weak gamma radiation from the thorium series. The results are tabulated below:

TABLE 3.5

Source	Counting rate: In 1.46 - 1.74 Mev	In 1.70 - 1.88 Mev
Vanadium	0.13 ± .02 cpm	d = .024 ± .02 cpm
Uranium	e = 16,294 cpm	f = 8,768 cpm

The quantity $(ed/f) = .044$ counts per minute gives some measure of the contribution of a possible uranium contaminant. Two values for the net vanadium sample activity in the energy range from 1.46 to 1.74 Mev are thus obtained by subtracting the calculated contribution due to the impurity from the vanadium sample counting rate:

$0.106 \pm .029$ counts per minute ..... C_{V1} (corrected for Th impurity)

$0.086 \pm .029$ counts per minute ..... C_{V2} (corrected for U impurity)

The specific activity of the 1.58 Mev gamma ray, S_V, for vanadium can be expressed in terms of the specific gamma ray activity of potassium, S_K, as follows:

$$S_V = \frac{C_V \, (MAGe_p e_d)_K}{C_K \, (MAGe_p e_d)_V} \, S_K$$

Where M_K = weight of K in KCl sample (37.55 grams)

M_V = weight of vanadium sample (186 grams)

A = the aborption correction needed to account for the fact that gammas interact with matter in three well-known ways.

At the energy considered the ratio of $A_K/A_V = 1$

G = geometrical factor-in this case the same for both the vanadium and potassium samples.

$(e_d)_K/(e_d)_V$ = ratio of the efficiency of the NaI crystal in detecting the gamma rays of energy 1.465 and 1.58 Mev.

= 1.03 for a 1 1/2 x 1 inch high NaI crystal with source removed 0.2 cms. from the crystal(40).

$(e_p)_K/(e_p)_V$ = the ratio of the photofraction of the two gammas here concerned. The photofraction of any gamma of energy W is the fraction of events taking place in the crystal

due to the gamma and that give rise to pulses in the photoline

$= 1.03$

S_K = the specific activity of K^{40} gamma activity. It is taken to be 3.4 ± 0.1 gamma quanta per second per gram of potassium(41)(27).

The specific activity S_V then becomes:

$S_{V1} < 12.69 \times 10^{-4}$ and $S_{V2} < 9.13 \times 10^{-4}$

1.58 Mev gamma quanta per second per gram of vanadium for C_{V1} and C_{V2}, respectively.

The partial decay constant, λ, and the partial half-life, t, for K capture in V^{50} to the first excited level in Ti^{50} at 1.58 Mev are then readily evaluated and are tabulated below:

$S_{V1} < 12.69 \times 10^{-4}$ gammas/sec./gm. of V ; $S_{V2} < 9.13 \times 10^{-4}$ gammas/sec./gm. of V.

$\lambda < 4.47 \times 10^{-23}$ seconds^{-1} $\lambda < 3.22 \times 10^{-23}$ seconds^{-1}

$t > 4.92 \times 10^{14}$ years $t > 6.8 \times 10^{14}$ years

For a transition energy of 1.58 Mev these half-lives yield $\log_{10}$ ft values of 23.24 and 23.38, respectively. The half-lives are written as inequalities in view of the uncertainty in the background enhancement factor, as well as of the fact that the corrections applied are somewhat arbitrary in nature. To determine them with more rigour would require that a comparison of the complete vanadium pulse height distribution spectrum be made with similar spectra from thorium and radium samples. By identifying similar features on the spectra and determining their relative intensities a more accurate correction factor might conceivably be arrived at. With the very low counting rate obtained from the vanadium sample such a procedure is not feasible.

The values obtained for the half-life of the decay of V^{50} to Ti^{50} by K capture are in general agreement with the theory and the values of the half-life for this mode of decay obtained by other workers. That the 1.58 Mev gamma ray has been detected conclusively is not certain. A different approach to the problem is proposed.

If the 1.58 Mev gamma from the excited level of Ti^{50} exists then its emission should be followed by the Ti K x-rays of energy 4.5 kev. A conicidence count of the 1.58 Mev gamma and the 4.5 kev K x-rays should then be possible. Using a large NaI(Tl) crystal to detect 1.58 Mev gamma rays and an unmounted CsI crystal, which is nonhygroscopic, to detect the soft K x-rays, with a thinly spread out source that could also serve as a reflector, the total absorption of the x-rays in the source could possibly be avoided. By putting both scintillation counters inside the lead shield the coincidence due to background should be minimized. A source enriched in V^{50} would increase the genuine coincidence counts. By doing a similar experiment with K^{40} the specific activity of the 1.58 Mev gamma transition in vanadium would be computable.

CHAPTER IV

TANTALUM 180

(i) Introduction:

The 8.3 hour activity of Ta^{180} has been known for about twenty years. It is produced in a number of different reactions: $Ta^{181}(n,2n)$, $Ta^{181}(\gamma,n)$, $Ta^{181}(p,pn)$, $W^{182}(\gamma,pn)$. A decay scheme has been proposed by Brown et al (52) and is shown below:

FIGURE 4.1

DECAY SCHEME OF TANTALUM 180

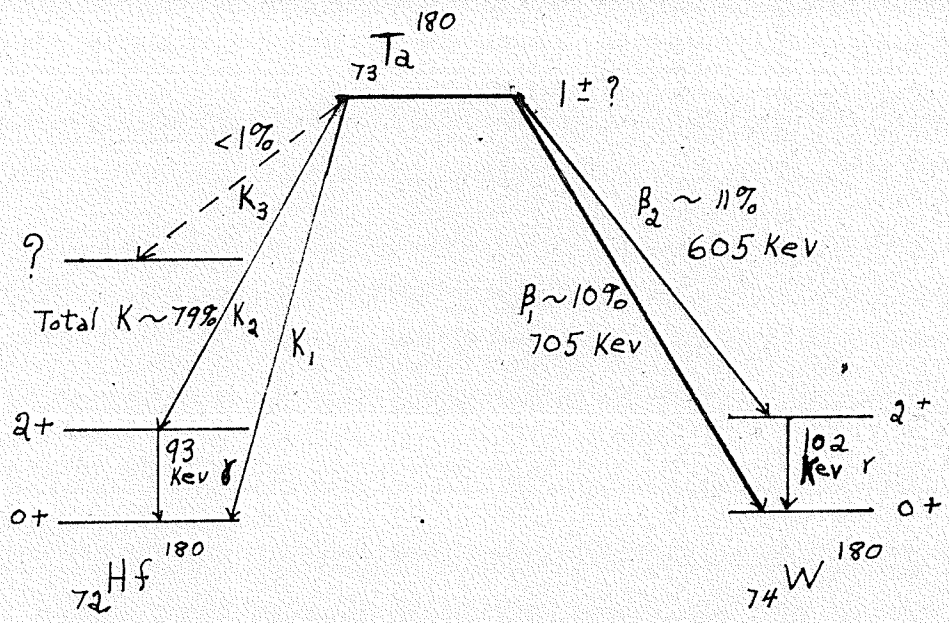

The $\log_{10}ft$ values of β_1 and β_2 are given as 6.8 and 6.5 respectively(52), thus classifying the transitions as first forbidden ($\Delta J=1$ (yes)), or possibly allowed but ℓ forbidden, in which case no parity change is involved. Since W^{180} is an even-even nucleus with ground state J=0+ and first excited level J = 2+ this implies that the 8.3 hour level of Ta^{180} has J=1 (±).

Recently (53) mass spectrographic evidence has been reported for

the presence of Ta^{180} as an isotope of terrestrially occurring tantalum, with an abundance of 0.0123% . Taken together with the adjacent isobars Hf^{180}(35.44%) and W^{180}(0.135%) Ta^{180} is the central member of a naturally occurring isobaric triad, of which at least one member should be radioactive. The radioactive member is most likely Ta^{180} because of its odd-odd character. Its low isotopic abundance supports this view. It follows then that the 8.3 hour activity of tantalum is proceeding from a metastable state of Ta^{180} since the ground state must have a half-life of the order of, or greater than, the age of the earth. The failure of previous workers to detect evidence for an isomeric transition from this state implies that the partial half-life for this mode of decay is long compared with 8.3 hours. Brown et al (52) postulate a weak ($<1\%$) K capture transition to a second excited level of Hf^{180} to explain the presence of a weak gamma ray component in the energy range 175 - 450 kev. Such a gamma ray could follow the excitation of the second excited level of Hf^{180} at 309 kev or alternatively it might be due to the isomeric transition proposed in the foregoing. Taking 1% as the relative intensity of this component one arrives at a minimum half-life of about 830 hours for the isomeric transition. This in turn implies some combination of low transition energy and high multipolarity for the transition. According to the shell model the neutron-proton configurations for the ground state of Ta^{180} may be taken to be $(g_{7/2}, p_{1/2})$ on the basis of the configurations for the odd Z nucleus Ta^{181} and the odd N nucleus Hf^{179}. Invoking Nordheim's weak coupling rule (54) this implies the ground state spin and parity of Ta^{180} is 3 or 4 (-) . In view of the probable assignment of J=1(-) for the 8.3 hour level this leads to the selection rules $\Delta J = 2$ or 3(no)

for the isomeric transition. The long half-life estimated in the foregoing mitigates in favour of $\Delta J=3$(no) leading to the proposal of $J=4(-)$ for the ground state of Ta^{180}.

On this basis the ground-ground state transitions between Ta^{180} and either Hf^{180} or W^{180} obey the selection rules $\Delta J=4$(yes) and are therefore third forbidden unique. Taking $\log_{10} ft=18$ as representative of this class of transitions, and assuming a transition energy of 700 kev for the negatron transition and 400 kev for the electron capture decay one arrives at half-lives of 5.0×10^{16} and 1.5×10^{17} years respectively, for these possible modes. Transitions to the first excited levels will obey the selection rules $\Delta J=2$(yes) and will be first forbidden unique with $\log_{10}$ ft between 7.4 and 9.9, and should certainly be observable, even for transition energies as low as 300 kev. It is noteworthy that these half-lives represent minimum values in view of the maximum transition energies taken. For a range of possible half-lives see the table below:

TABLE 4.1

HALF-LIVES

Mode of decay	Energy of transition	$\log_{10}$ ft	Half-life
Negatron emission	600	7.4 - 9.9	2.0×10^7 to 6.3×10^8 years
K-capture	300	7.4 - 9.9	7.9×10^5 to 2.5×10^8 years

Eberhardt et al(55) have examined various tantalum ores in a search for substantial quantities of W^{180} which should follow the

negatron decay of Ta^{180}, and have established a minimum half-life of 10^{12} years for this mode of decay in contrast to the foregoing argument.

A similar case to that proposed for Ta^{180} is the one of Lu^{176} where the ground state has a total half-life of 4×10^{10} years for negatron emission and for K capture, while the first excited level has a half-life for negatron emission of 3.7 hours. No evidence for the isomeric transition $Lu^{176*} \rightarrow Lu^{176}$ has been advanced. This is to be expected since Lu^{176*} has $J=1(\pm)$ and Lu^{176} has $J \geq 7$. According to the shell model Lu^{176}($Z=71, N=105$) should have the proton configuration of $Lu^{175}(g_{7/2})$ and the neutron configuration of $Hf^{177}(p_{1/2}, p_{3/2})$ as in the case of Ta^{180}. Klinkenberg(56) has shown that in the case of Lu^{176} the odd proton is in the $6h_{11/2}$ state and the odd neutron is in the $7i_{13/2}$ state and proposes the assignment $J=10(-)$ for the ground state without excluding the possibility of $J=9$ or 11 . He suggests as an explanation for this departure from the usual shell model level scheme the presence of a large quadrupole moment. The recent unified model of Bohr and Mottelson (57) predicts a large quadrupole moment for isotopes well removed from closed shells as are Lu^{176} and Ta^{180}, on the basis of large core deformations. With strong coupling between the extra nucleons and the deformed core departures from the strict single particle model are to be expected. It is thought then that the spin of the ground state of Ta^{180} might also arise from the higher angular momentum configuration $(h_{11/2}, i_{13/2})$ and is of a magnitude comparable to that of Lu^{176}.

A clearer picture of the static properties of Ta^{180} must await further experimental data. The present investigation is an attempt to detect the gamma radiation which should follow the decay of Ta^{180}

to any of the excited levels of either Hf^{180} or W^{180}.

(ii) Apparatus and Experimental Procedure:

In attempting to detect the natural radioactivity of Ta^{180}, the scintillation spectrometer described in Chapters 2 and 3 was used. In the hope of being able to separate the expected 93 kev gamma ray proceeding from the first excited level to the ground state of Hf^{180} from the expected 102 kev gamma ray from the first excited level of W^{180} to its ground state, a 1 1/4 x 1 1/2 inch NaI(Tl) crystal, mounted in the normal fashion in an Al can, was used. Coupled to the K1190 photomultiplier tube the resolution of the 662 kev gamma ray from Cs^{137} was found to be 9.6% . Two sources of Ta^{180} were obtained. Photographic analysis showed that the first sample tried, 75 grams of Ta_2O_5 obtained from Fisher Scientific Company, was contaminated with radioactive products from the Thorium and Uranium series. A pulse height analysis supported this fact. For the second sample, 50 grams of Tantalum powder obtained from Johnson, Matthey & Co., Limited, were used. Spectrographical estimates of the quantities of the impurities present were made by the producers and are given below:

TABLE 4:2

Estimates of Impurities in Tantalum Powder

Element	Parts per Million
Iron	30
Niobium	10
Silicon	10
Magnesium	10
Nickel	5

TABLE 4.2 Cont'd

Element		Parts per Million
Aluminium		2
Calcium		1
Sodium	less than	1

Elements specifically sought but not detected:

Ag, As, Au, Ba, Be, Cd, Co, Cr, Ga, Ge, Hg, In, Ir, K, Li, Mn, Mo, Os, Pb, Pd, Pt, Rb, Rh, Ru, Sb, Sn, Sr, Te, V, W, Zn, Zr.

These 50 grams of Tantalum powder were packed into a plastic container fitted snugly over the crystal so that the powder covered the cylindrical wall of the crystal to a thickness of about 1 mm. Photographic analysis (48 hour exposure) revealed some weak activity of energy around 65 kev. A wide channel pulse height distribution analysis showed no net activity above 400 kev that was not within the statistical error of the background counting rate. A narrow channel pulse height distribution analysis between 40 and 360 kev was undertaken and a histogram of the net activity of the Tantalum powder in this energy interval is given in figure 4.1 . An analysis of the histogram verifies the presence of radiation of energy around 65 kev and possibly indicates some activity between 90 and 100 kev.

(iii) Interpretation of Results:

Whether the expected decay of Ta^{180} proceeds by negatron emission to W^{180} or by electron capture to Hf^{180}, unless the transition is to the ground state, a gamma ray pulse height distribution should yield evidence of the detection of either a 93 kev or 102 kev gamma ray as well as a K x-ray of either W or Hf depending on the mode of decay. The experimental distribution (figure 4.2) shows a prominent feature at around 64 kev. It is tempting to interpret this as a superposition

FIGURE 4.2

HISTOGRAM OF TANTALUM 180

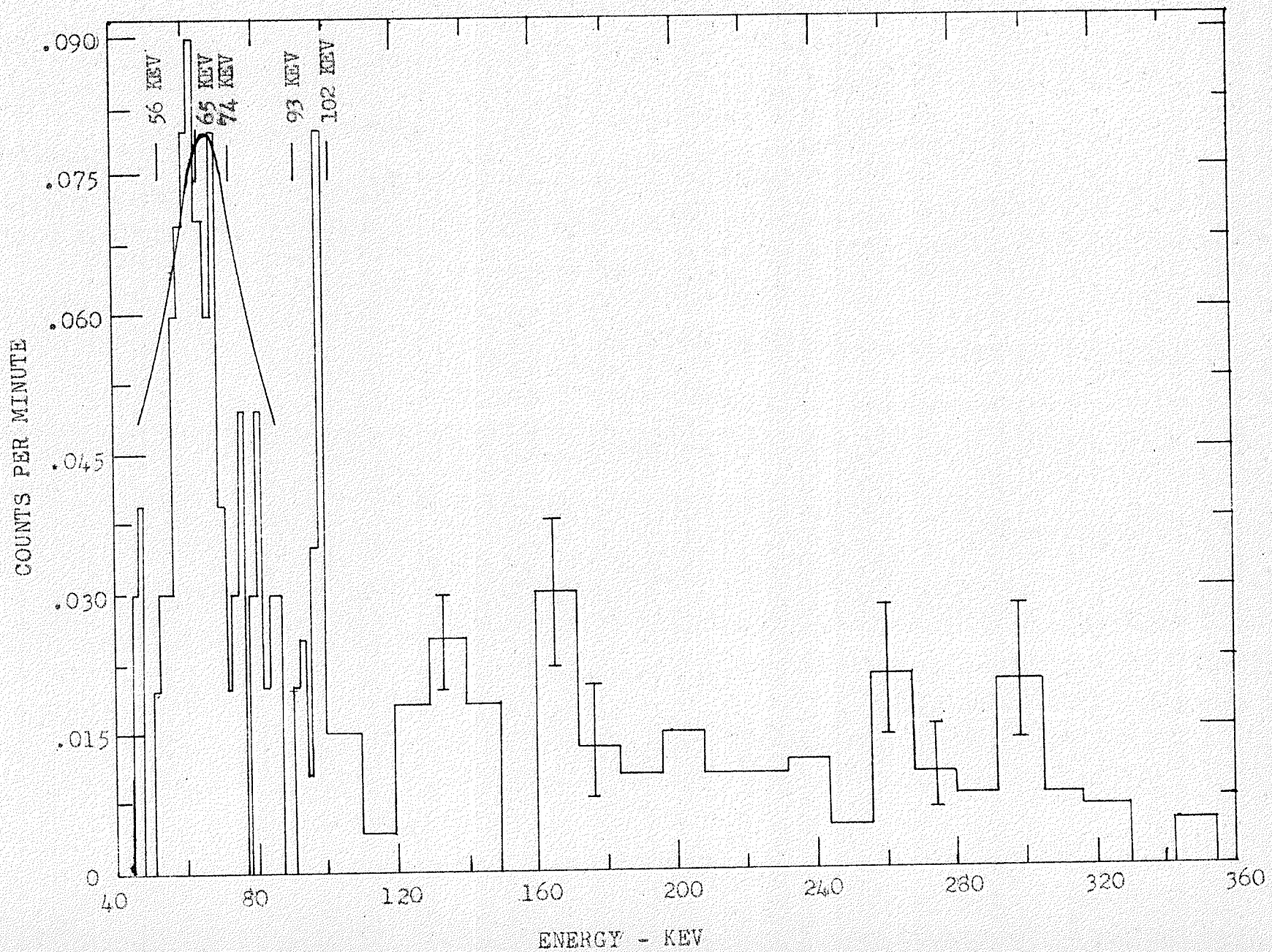
.090
.075
.060
.045
.030
.015
0
COUNTS PER MINUTE
56 KEV
65 KEV
74 KEV
93 KEV
102 KEV
40
80
120
160
200
240
280
320
360
ENERGY - KEV

of K x-ray pulses plus the escape peak of a gamma ray of energy about 100 kev, and in view of the limited statistical accuracy (about 10%) this interpretation cannot be rejected conclusively. There are, however, a number of strong arguments against it. The width of the superimposed distribution of the 67.4 kev calibration line indicates that the prominent feature on the distribution is not a superposition line, unless the superimposed components are close together on the energy scale, or unless there is one prominent line near 65 kev with the other components of a much smaller intensity. In the figure there is indicated the expected location of the K x-ray (56 kev), the escape peaks for the 93 kev gamma ray (65 kev) and the 102 gamma ray (74 kev), the photolines for the 93 kev and 102 kev gamma rays. It is clear that not all these features are present in the observed distribution with equal intensity, since in this event the distribution should be much broader. The most plausible explanation is that the feature arises from a superposition of the 56 kev K x-ray, the 65 kev escape peak for the 93 kev gamma ray and the photoline for the latter gamma ray. That this explanation is not likely can be seen from a consideration of its implication. If the 93 kev level in Hf^{180} is being excited by K-capture, there should be 9.3 K x-rays for every 10 disintegrations since the K shell fluorescence yield of Hf is 93%. The 93 kev level will be de-excited in an E2 transition with a large internal conversion coefficient. The tables of internal conversion coefficients are unfortunately not complete so that a reliable estimate of the relative number of gamma rays and K x-rays following internal conversion cannot be made. For the sake of the argument we use the K shell (Z=72) conversion coefficient α_2 for 150 kev E2 radiation as given by

Rose et al(60), as indicative of the order of magnitude. For the energy of 150 kev α_2=.34; the actual value will be higher. The expectations for this case are summarized in the table below:

TABLE 4.3

Relative Number of Gamma and K x-rays

For 10 K-capture events --- 9.3 K x-rays due to K-capture

$\geq$ 2.4 K x-rays due to internal conversion

$\leq$ 7.1 93 kev gamma rays of which only 0.2 will give rise to an escape peak.

For such a mode of decay one should expect to find a x-ray line **of about two times** the intensity of a line at 93 kev, with only a **feeble** indication, if any, of the escape peak. The **predictions** for any of the other possible modes of decay are even less in accord with the observed distribution. In view of this consideration it is concluded that the Tantalum sample employed in the investigation is contaminated with a radioactive impurity. This conclusion is further corroborated by the presence of higher energy gamma radiation out to about 350 kev.

If the observed counting rate of 0.48 $\pm$.10 counts per minute between 80 and 110 kev is considered as the activity in the photoline of a gamma ray transition from the first excited level of either Hf^{180} or W^{180}, then the **specific** activity for this mode of decay may be calculated. The photoline counting rate, C, for a gamma ray of energy E_γ from a source of mass M and specific activity S may be expressed as:

$$C = SMe_d e_p AGK \quad , \quad \text{-----(4.1)}$$

where: e_d = the crystal detection efficiency for E_γ, that is, the probability that a gamma ray of energy E_γ will undergo any kind of interaction with the crystal

$e_d \approx 100\%$ for a gamma ray of energy 100 kev (58)

e_p = the photofraction, or the fraction of events occasioned in the crystal by E_γ that yield pulses in the photoline.

= 95% for a gamma ray of energy 100 kev (58)

G = geometrical factor. In the present experiment the geometry was estimated roughly to be .40 .

X = the fraction of the transitions from the ground state of Ta^{180} to the first excited level of either Hf^{180} or W^{180} which give rise to gammas of energy 93 kev or 102 kev.

= .71 for the 93 kev gamma ray, and will be of the same order of magnitude for the 102 kev gamma ray.

A = an attenuation resulting from self- absorption in the source and absorption in the material interposed between the source and the sensitive volume of the detector.

For a monoenergetic collimated beam of gamma rays of intensity I_o incident on a target of thickness d, the transmitted intensity I is given by the equation

$$I = I_o e^{-\mu d} \qquad \text{----(4.2)}$$

where μ is the mass absorption coefficient in cm^2-gms^{-1} if d is in units of gm-cm^{-2}. For self-absorption in the source for normal emergence

$$A = I/I_o = (1 - e^{-\mu d})/\mu d \qquad \text{----(4.3)}$$

Values of μ for Ta, MgO, and Al are given in the following table:

TABLE 4.4

Mass Absorption Coefficient μ - cm^2-gm^{-1}

E_γ (Kev)	Ta	MgO	Al
100	4.36	.163	.169

Absorption by the plastic container and the layer of air interposed between the source and crystal has been neglected.

The thickness, d, for the MgO reflector and the Aluminum can were taken to be 0.89 gm/cm^2 and 0.22 gm/cm^2, respectively(27). To calculate d for the source the total area of the curved surface of the right cylinder lying midway between the inner and outer edges of the source was calculated and divided into the source weight. For a calculated area of 47.8 cm^2, the corresponding thickness is 1.05 gm/cm^2 . The value of A for the absorbers, MgO and Al, and the self-absorber, Ta, are then readily calculated from equations 4.2 and 4.3 , respectively. Values for μd and A, the attenuation, appear in the following table:

TABLE 4.5

Values of μd and A

	μd			A		
E_γ(Kev)	Ta	MgO	Al	Ta	MgO	Al
100	4.58	.142	.037	.21	.869	.965

The overall value for the attenuation then becomes 0.17

Alternatively, the attenuation factor was obtained by considering the analytical function, developed by Mulholland(59) which, for 2π geometry, expresses the fraction of emitted photons which actually emerge from a layer of thickness t and traverse an absorber of thickness T, where the thicknesses are measured in multiples of the mean free path for each substance. For t=4.58 and T = .179 the attenuation factor was determined from curves of t vs. T to be 0.083 . The value

of 0.063 for the attenuation is for the general case where the angle of emergence need not be normal, and may therefore, be too conservative. On the other hand, the value of 0.17 determined for normal emergence may be somewhat too optimistic. A mean of the two values was taken as the value of A. Therefore A=0.13 .

From equation 4.1 the expression for the specific activity S can be written as:

$$S = C / M e_d e_p A G X \qquad \text{--------(4.4)}$$

where: $C = 5.5 \times 10^{-3}$ counts per second

$e_d = 1$

$e_p = .95$

$G = .40$

$A = .13$

$X = .71$

$M = 50$ gm

Therefore, $S = 3.1 \times 10^{-3}$ gamma quanta per second per gram of Tantalum, where the energy of the gamma ray is 93 kev or 102 kev. The decay constant, λ, was then readily calculated to be 7.6×10^{-21} seconds^{-1}, corresponding to a half-life of 2.9×10^{12} years, which agrees with the minimum half-life for negatron emission of 10^{12} years established by Eberhardt et al(65). With an end-point energy of 600 kev for negatron emission and an end-point energy of 400 kev for K-capture, the respective $\log_{10}$ ft values are 21 and 20.7 in contrast to 7.4 - 9.9 proposed in the introduction. A $\log_{10}$ ft value of 21 corresponds to a fourth forbidden or possibly to a third forbidden unique transition. Even if only a transition energy of 200 kev is assumed between the ground state of Ta^{180} and the first excited levels of W^{180} and Hf^{180}, the associated

$\log_{10}$ ft values are still 19.5 and 20.4 , respectively, thus indicating that the foregoing classification is not altered. It is noteworthy that in view of the fact that the transition energy of 200 kev between the ground state of Ta^{180} and the first excited levels of W^{180} and Hf^{180} represents almost the minimum possible, the corresponding $\log_{10}$ ft values are therefore a minimum. It therefore seems almost certain that the spin of the ground state of Ta^{180} is greater than 4 as proposed on the basis of assuring the neutron-proton configurations for the ground state of Ta^{180} to be $(g_{7/2}, p_{1/2})$. A greater spin for the ground state of Ta^{180} is obtained if the proton-neutron configurations are assumed to be $(h_{11/2}, i_{13/2})$. The forbiddenness of the transition from the isomeric state to the ground state of Ta^{180} is then correspondingly increased.

ACKNOWLEDGEMENTS

The writer wishes to express his sincere thanks to Dr. W.E. Turchinetz for his interest and invaluable direction; to Dr. K.I. Roulston for advice in electronic problems; to Dr. H. Blondal of the Medical College, for supplying the iodine 131; to Dr. G.M. Lewis for the rubidium iodide thallium activated crystal; and to Mr.C.J.Kubin and Mr. D. Hewuson for their cooperation in the construction and maintenance of the equipment.

The assistance of the National Research Council of Canada in the form of a grant is gratefully acknowledged.

BIBLIOGRAPHY

1. M.E. Rose Chapter IX Beta and Gamma Spectroscopy - edited by Kai Siegbahn
2. Chapter 111 Introductory Nuclear Physics - D. Halliday
3. Chapter X111 Theoretical Nuclear Physics - Blatt and Weisskopf
4. Chapter XV11 The Atomic Nucleus - Robley D. Evans
5. Page 95, Halliday, (See reference 2)
6. Page 277 ff Chapter 1X Siegbahn (See reference 1)
7. Page 280 ff Chapter 1X Siegbahn (See reference 1)
8. H.M. Mahmoud and E.J. Konopinski Phys. Rev. 88 (1952) 1266
9. E.J. Konopinski Chapter X Siegbahn (See reference 1)
10. Page 303 Chapter X Siegbahn (See reference 1)
11. M.E. Rose, C.L. Perry, and N.M. Dismuke, Oak River National Laboratory, Report No: 1459 (1953)
12. W.T. Leland, Phys. Rev. 76, 1722, (1949)
13. Blatt J.M. Phys. Rev. 89 No: 1 Jan. 1953, Page 83
14. E. Feenberg and G. Trigg Rev. Mod. Phys. 22 (1950) 399
15. J.J. Thomson, Phil. Mag. 10 584 (1905)
16. A. Hemmendinger, Phys. Rev. 51 1052 (1937)
17. A.O. Nier, Phys. Rev. 79 450 (1950)
18. S. Eklund, Ark. f. Mat. Astr. Physik, Vol. 33a, 60 (1946)
19. O. Haxel, F.G. Houtermans, and M. Kemmerich, Phys. Rev. 74, 1886 (1948)
20. Curran, Dixon, and Wilson, Phys. Rev. 84, 151, (1951)
21. M.H. MacGregor and M.L. Wiedenbeck, Phys. Rev. 86, 420 (1952)
22. Sawyer and Wiedenbeck, Phys. Rev. 79, 790 (1950)
23. G.M. Lewis, Phil. Mag. 43, 1070 (1952)
24. Morita, Fujita, and Yamada, Prog. of Theor. Phys. 10 No: 6, 630

Dec. 1953

25. The Beta Spectrum of Rb^{87} and the Beta-Decay Interaction July 3, 1956 - Private Communication from Charles E. Goodman

26. Proceedings of the Conference on Nuclear Processes in Nature, - T.P. Kohman Pages 10 - 20, (1954)

27. W. Turchinetz, Ph.D. Thesis, 1955, University of Manitoba

28. W. Turchinetz, M. Sc. Thesis, 1953, University of Manitoba

29. G.L. Davis and L.T. Aldrich, Bull. Geol. Soc. Am. 64, 379 (1953)

30. H. Selig, Thesis, Carnegie Inst. Tech. (1954) Doctoral Dissertation N.Y.O. - 6626

31. J Heintze, Z. Natur f. 109, 77 (1955)

32. F.C. Strome, Jr., Dissertation Abstract 14, 699 (1954)

33. G.S. Goldhaber Phys. Rev. 90, 587 (1953)

34. Private communication from C.E. Miller, Argonne National Laboratory

35. Nucleonics Vol. 13 No: 10, Oct. 1955 Page 89

36. P.R. Bell Page 150 Chapter 5 Beta and Gamma Spectroscopy (See reference 1)

37. G.F. Pieper, Phys. Rev. 88, 1299 (1962)

38. Meller's Modern Inorganic Chemistry, Page 794 Revised Edition Longmans, Green and Co. (1951)

39. Rev. Mod. Phys., 25, No: 2, 469 (1953)

40. Figure 18, Page 154, Beta and Gamma Spectroscopy - Siegbahn (See reference 1)

41. Endt and Kluyver, Rev. Mod. Phys., 26, 95 (1954)

42. M.A. Preston and Kailash Kumar, Phys. Rev. 102, 1347 (1956)

43. C. Kikuchi, M.H. Sirvetz and V.W. Cohen, Phys. Rev. 88, 142 (1952)

44. W.H. Johnson, Phys. Rev. 87, 166 (1952)

45. Appendix 11. Page 875 Siegbahn (See reference 1)

46. L.H. Ahrens, Bull. Geol. Soc. Am. 60, 217 (1949)

L.H. Ahrens and L.H. Gorfinkle, Nature 166, 149 (1950)

L.H. Ahrens and A.M. MacGregor, Science 114, 64 (1951)

47. G.W. Wetherill, L.T. Aldrich, G.R. Tilton, and G.L. Eavis, Bull. American Phys. Soc., Series 11 Vol. 1, No: 1, Page 31

48. R.G. Johnson, O.E. Johnson, and L.M. Langer, Phys.Rev. 102 ,No: 4 1142, (1956)

49. J.P. Palmer and L.J. Laslett , U.S. Atomic Energy Commission Bulletin ISC -174 (1950)

50. M. Yamada , Progr. of Theor. Phys. Vol 9 #3 , March, 1953

51. W. Libby, Figure 22, Page 22 Siegbahn (See reference 1)

52. H.N.Brown, W.L. Bendel, F.J.Shore, and R.A.Becker, Phys. Rev. 84, 292 , (1951)

53. F.A. White, T.L. Collins, Jr. and F.M. Rourke , Phys.Rev. 97, 566 (1955)

54. L.W. Nordheim, Rev. Mod. Phys. 23 , 322, (1951)

55. P. Eberhardt, J.Geiss, F.G. Houtermans, Z. Naturf., 10a, 796, (1955)

56. P.F.A. Klinkenberg, Physica 17 , 715, (1951)

57. A.Bohr and B.R. Mottelson, Chapter XVII Siegbahn (See reference 1)

58. P.R. Bell, Chapter V Siegbahn (See reference 1)

59. G.I. Mulholland, Doctoral Thesis, Carnegie Institute of Technology (1952)

60. M.E.Rose, Appendix IV Page 904 Siegbahn (See reference 1)